TKK Dissertations 156
Espoo 2009

PATHWAYS TOWARD CONTROLLED ASSEMBLY OF FUNCTIONAL POLYMER-BASED NANOSTRUCTURES

Doctoral Dissertation

Ari Laiho

Helsinki University of Technology
Faculty of Information and Natural Sciences
Department of Applied Physics

TKK Dissertations 156
Espoo 2009

PATHWAYS TOWARD CONTROLLED ASSEMBLY OF FUNCTIONAL POLYMER-BASED NANOSTRUCTURES

Doctoral Dissertation

Ari Laiho

Dissertation for the degree of Doctor of Science in Technology to be presented with due permission of the Faculty of Information and Natural Sciences for public examination and debate in Auditorium AS1 at Helsinki University of Technology (Espoo, Finland) on the 3rd of April, 2009, at 12 noon.

Helsinki University of Technology
Faculty of Information and Natural Sciences
Department of Applied Physics

Teknillinen korkeakoulu
Informaatio- ja luonnontieteiden tiedekunta
Teknillisen fysiikan laitos

Distribution:
Helsinki University of Technology
Faculty of Information and Natural Sciences
Department of Applied Physics
P.O. Box 5100
FI - 02015 TKK
FINLAND
URL: http://tfy.tkk.fi/
Tel. +358-9-451 3153
Fax +358-9-451 3155
E-mail: ari.laiho@tkk.fi

ISBN 978-951-22-9814-3
ISBN 978-951-22-9815-0 (PDF)
ISSN 1795-2239
ISSN 1795-4584 (PDF)
URL: http://lib.tkk.fi/Diss/2009/isbn9789512298150/

TKK-DISS-2579

Picaset Oy
Helsinki 2009

HELSINKI UNIVERSITY OF TECHNOLOGY
P. O. BOX 1000, FI-02015 TKK
http://www.tkk.fi

ABSTRACT OF DOCTORAL DISSERTATION

Author Ari Laiho

Name of the dissertation

Pathways toward controlled assembly of functional polymer-based nanostructures

Date of manuscript 20.01.2009 | Date of the dissertation 03.04.2009

☐ Monograph ☒ Article dissertation (summary + original articles)

Faculty Faculty of Information and Natural Sciences
Department Department of Applied Physics
Field of research Soft condensed matter physics
Opponent Prof. Ullrich Steiner, University of Cambridge (UK)
Supervisor Acad. Prof. Olli Ikkala, Helsinki University of Technology

Abstract

This thesis deals with a common drawback that is often encountered in self-assembled nanostructured soft matter. Even though spontaneous self-assembly can be used to create diverse nanostructures, the structures, as such, are typically polydomain, consisting of locally ordered small domains that lack mutual orientation and/or long range correlation. As a result, the material remains macroscopically isotropic and disordered. The aim here is to explore feasible ways, on one hand, to control the assembly and, on the other hand, to obtain macroscopically anisotropic materials and functions.

We show the first example of how charge-transfer complexation between C_{60} fullerenes and electron-donating units of block copolymers can enable control of the morphology and properties of fullerene based materials. We also study the alignment of randomly oriented domains of nanostructured material over macroscopic length scales by using a real-time rheo-optical apparatus in combination with more detailed *ex-situ* structural characterization. Alignment of randomly oriented domains is not only useful for obtaining macroscopically anisotropic materials and functions but it can also be a prerequisite for detailed characterization of the local structures. This aspect is demonstrated for hierarchical liquid crystalline (LC) diblock copolymer structures which, upon inducing shear alignment, exhibit coexistence of two orthogonal orientations of the LC phase within the copolymer lamellae. Furthermore we demonstrate that ionic complexes forming a columnar LC phase can be efficiently aligned within polymer blends upon shearing, taken that the matrix polymers have sufficiently high molecular weight. This concept allows a simple route for macroscopically aligned nanocomposites with conjugated columnar LC functional additives. Finally, control of the nanoscale morphology in polymer/fullerene nanocomposite thin film devices is shown to allow tuning of the electrical switching that can enable construction of a memory unit. The working principles of such thin film organic memory devices have remained debated and the first systematic approach is here undertaken to tailor the active material composition and to study the morphology vs. functionality relationship.

Keywords: self-assembly, shear alignment, block copolymer, fullerene, organic electronics

ISBN (printed) 978-951-22-9814-3 | ISSN (printed) 1795-2239
ISBN (pdf) 978-951-22-9815-0 | ISSN (pdf) 1795-4584
ISBN (others) | Number of pages 50 p. + app. 45 p.
Publisher Helsinki University of Technology, Department of Applied Physics
Print distribution Helsinki University of Technology, Department of Applied Physics
☒ The dissertation can be read at http://lib.tkk.fi/Diss/2009/isbn9789512298150/

TEKNILLINEN KORKEAKOULU PL 1000, 02015 TKK http://www.tkk.fi	VÄITÖSKIRJAN TIIVISTELMÄ

Tekijä Ari Laiho

Väitöskirjan nimi

Menetelmiä funktionaalisten polymeerinanorakenteiden morfologian hallintaan

Käsikirjoituksen jättämispäivämäärä 20.01.2009	Väitöstilaisuuden ajankohta 03.04.2009

☐ Monografia ☒ Yhdistelmäväitöskirja (yhteenveto + erillisartikkelit)

Tiedekunta	Informaatio- ja luonnontieteiden tiedekunta
Laitos	Teknillisen fysiikan laitos
Tutkimusala	Pehmeän tiiviin aineen fysiikka
Vastaväittäjä	Prof. Ullrich Steiner, University of Cambridge
Työn valvoja	Akat. Prof. Olli Ikkala, Teknillinen korkeakoulu

Tiivistelmä

Tämä väitöskirja käsittelee itsejärjestyville pehmeille materiaaleille tyypillistä ongelmaa: spontaania itsejärjestymistä voidaan käyttää moninaisten nanorakenteiden valmistukseen, mutta muodostuvat rakenteet ovat tyypillisesti vain paikallisesti hyvin järjestyneitä ja rakennealueiden keskinäinen orientaatio on satunnaista. Tämän seurauksena materiaali on makroskooppisessa skaalassa isotrooppista ja epäjärjestynyttä. Työn tavoitteena on kehittää menetelmiä, joilla voidaan ohjata nanorakenteiden muodostumista sekä saada aikaan makroskooppisessa skaalassa anisotrooppisia materiaaleja ja ominaisuuksia.

Työssä osoitetaan ensimmäisen kerran, miten C_{60}-fullereenin ja elektroni-donoreita sisältävän lohkopolymeerin välistä varauksenvaihtoreaktiota voidaan käyttää fullereenipohjaisten materiaalien morfologian ja ominaisuuksien hallintaan. Lisäksi työssä tutkitaan erilaisten paikallisten nanorakenteiden orientoimista virtauskentässä käyttämällä hyväksi työssä kehitettyä reo-optista mittauslaitteistoa. Rakennealueiden orientoiminen ei ole tärkeää pelkästään anisotrooppisten materiaalien ja ominaisuuksien saavuttamiseksi, vaan se on usein myös edellytys paikallisten nanorakenteiden yksityiskohtaiselle tutkimiselle. Tätä näkökulmaa havainnollistetaan nestekiteisillä lohkopolymeerirakenteilla, joissa virtauskenttäorientaation osoitetaan johtavan kahteen ortogonaaliseen nestekidefaasirakenteeseen. Työssä esitetään lisäksi menetelmä ionisesti itsejärjestyvien, kolumnaarisen nestekidefaasin muodostavien rakenteiden orientoimiseksi perustuen ionisten kompleksien ja korkean molekyylipainon polymeerin muodostaman seoksen orientointiin virtauskentässä. Menetelmää voidaan yleisesti käyttää konjugoituja kolumnaarisia nestekiteitä sisältävien nanokomposiittien orientoimiseksi. Lopuksi osoitamme, kuinka nanoskaalan morfologiaa muokkaamalla voidaan hallita polymeeri/fullereeni nanokomposiitista valmistettavien ohutkalvolaitteiden sähköisiä ominaisuuksia. Tällaisten muistiyksiköiksi soveltuvien laitteiden toimintaperiaatteet ovat yhä kiisteltyjä ja tässä työssä pyritäänkin esittämään menetelmiä laitteiden toiminnan ohjaamiseen ja kartoittamaan morfologian ja toiminnallisuuden välisiä riippuvuussuhteita.

Asiasanat: itsejärjestyminen, virtauskenttäorientaatio, lohkopolymeeri, fullereeni, orgaaninen elektroniikka

ISBN (painettu)	978-951-22-9814-3	ISSN (painettu)	1795-2239
ISBN (pdf)	978-951-22-9815-0	ISSN (pdf)	1795-4584
ISBN (muut)		Sivumäärä	50 s. + liit. 45 s.

Julkaisija Teknillinen korkeakoulu, Teknillisen fysiikan laitos

Painetun väitöskirjan jakelu Teknillinen korkeakoulu, Teknillisen fysiikan laitos

☒ Luettavissa verkossa osoitteessa http://lib.tkk.fi/Diss/2009/isbn9789512298150/

Preface

The research reported in this thesis has been carried out in the Molecular Materials group, Department of Applied Physics at the Helsinki University of Technology. I am especially grateful to my thesis supervisor, Acad. Prof. Olli Ikkala, for not only providing the excellent research facilities but also for his support and encouragement and for being the endless source of new fancy ideas.

I wish to express my sincere gratitude to the members of the research groups of Prof. Ronald Österbacka from Åbo Akademi University, Dr. Charl Faul from the University of Bristol and Dr. Henrik Sandberg from the Technical Research Centre of Finland (VTT) for a superb collaboration. I want to thank all the co-authors for co-operation and discussions, especially Dr. Himadri Majumdar and MSc Jayanta Baral, whose contribution has been invaluable. I am most indebted to Prof. Janne Ruokolainen and MSc Antti Nykänen for introducing me to the exciting field of electron microscopy. Prof. Kell Mortensen (University of Copenhagen) and Prof. Ritva Serimaa (University of Helsinki) are gratefully acknowledged for the swift pre-examination of the thesis manuscript.

Completing the thesis would not have been as enjoyable without the inspiring, encouraging and enthusiastic working environment that flourishes in the Molecular Materials group, thanks to all past and present members. Especially, I wish to thank Antti Nykänen, Antti Soininen, Arri Priimägi, Mauri Kostiainen, Panu Hiekkataipale and Robin Ras.

The research reported in this thesis has been funded by the European Science Foundation (EUROCORES programme on Self-Organized NanoStructures), Academy of Finland (Centre of Excellence of Finnish Academy, Bio- and Nanopolymers Research Group, 77317) and the Finnish Funding Agency for Technology and Innovation (TEKES, FinNano Programme). In addition to the financial support from the preceding funding agencies, personal grants from Emil Aaltonen foundation, Vilho, Yrjö and Kalle Väisälä foundation and the Foundation of Technology are gratefully acknowledged.

Finally, I thank my family and friends for all the support and encouragement. My warmest thanks go to my wife Johanna for her love, support and patience and to our son Hannes who has supported me in his own attractive way.

Espoo, March 2009

List of Publications

List of Publications included in the thesis

This thesis consists of an overview and of the following Publications which are referred to in the text by their Roman numerals.

I A. Laiho, R.H.A. Ras, S. Valkama, J. Ruokolainen, R. Österbacka, and O. Ikkala, *Control of Self-Assembly by Charge-Transfer Complexation of C_{60} Fullerene to Electron Donating Units of Block Copolymers*, Macromolecules **39**, 7648 (2006). *Link*

II A. Laiho and O. Ikkala, *A rheo-optical apparatus for real time kinetic studies on shear-induced alignment of self-assembled soft matter with small sample volumes*, Review of Scientific Instruments **78**, 015109 (2007). *Link*

III A. Laiho, P. Hiekkataipale, J. Ruokolainen and O. Ikkala, *Coexisting Parallel and Perpendicular Orientations of Smectic Layers within Copolymer Lamellae in a Shear Aligned Liquid Crystalline Diblock Copolymer*, submitted to Macromolecular Chemistry and Physics, Helsinki University of Technology Publications in Engineering Physics, Report TKK-F-A856 (2009).

IV A. Laiho, B. Smarsly, C.F.J. Faul and O. Ikkala, *Macroscopically Aligned Ionic Self-Assembled Perylene-Surfactant Complexes within a Polymer Matrix*, Advanced Functional Materials **18**, 1890 (2008). *Link*

V J.K. Baral, H.S. Majumdar, A. Laiho, H. Jiang, E.I. Kauppinen, J. Ruokolainen, O. Ikkala and R. Österbacka, *Organic memory using [6,6]-phenyl-C_{61} butyric acid methyl ester (PCBM): morphology, thickness and concentration dependence studies*, Nanotechnology **19**, 035203 (2008). *Link*

VI A. Laiho, H.S. Majumdar, J.K. Baral, F. Jansson, R. Österbacka and O. Ikkala, *Tuning the electrical switching of polymer/fullerene nanocomposite thin film devices by control of morphology*, Applied Physics Letters **93**, 203309 (2008). *Link*

List of other publications

- P. Pulkkinen, J. Shan, K. Leppänen, A. Känsäkoski, A. Laiho, M. Järn and H. Tenhu, *ACS Appl. Mater. Interfaces* **1**, 519 (2009).
- A. Laiho, J.K. Baral, H.S. Majumdar, D. Tobjörk, J. Ruokolainen, R. Österbacka and O. Ikkala, *Mater. Res. Soc. Symp. Proc.* **1071**, 1071-F04-04 (2008).
- R. Ramani, S. Hanski S., A. Laiho, R. Tuma, S. Kilpeläinen, F. Tuomisto, J. Ruokolainen, O. Ikkala, *Biomacromolecules* **9**, 1390 (2008).
- A. Soininen, S. Valkama, A. Nykänen, A. Laiho, H. Kosonen, R. Mezzenga and J. Ruokolainen, *Chem. Mater.* **19**, 3093 (2007).
- S. Valkama, T. Ruotsalainen, A. Nykänen, A. Laiho, H. Kosonen, G. ten Brinke, O. Ikkala, J. Ruokolainen, *Macromolecules* **39**, 9327 (2006).
- H.S. Majumdar, J.K. Baral, A. Laiho, J. Ruokolainen, O. Ikkala and R. Österbacka, *Adv. Mater.* **18**, 2805 (2006).

Author's contribution

The author has contributed significantly to planning, implementation, analysis, interpretation and reporting at all stages of the research reported in this thesis. The author has written the first versions of Publications **I**-**IV** and **VI** and the parts dealing with structural analysis and spectroscopy of the devices in Publication **V**. All of the experimental work covered in this thesis has been carried out by the author with the following exceptions: infrared spectroscopy in Publication **I** was done by Dr. Robin Ras (TKK), wide-angle X-ray scattering in **IV** by Prof. Bernd Smarsly (Justus Liebig Universität Gießen), synthesis of the ionic complexes in **IV** by Dr. Charl Faul (University of Bristol), energy dispersive X-ray spectroscopy in **V** in collaboration with Dr. Hua Jiang (TKK), and final fabrication of the devices including the electrical measurements in **V** and **VI** by MSc Jayanta Baral (Åbo Akademi University). The author has designed, constructed and tested the rheo-optic setup reported in Publication **II**.

The author has also presented the results covered in this thesis at several international conferences.

Contents

1 Introduction

– when we have some control of the arrangement of things on a small scale we will get an enormously greater range of possible properties that substances can have –

Richard P. Feynman (1918-1988)

In the past decades, Feynman's vision of controlling *the arrangement of things on a small scale* has been fulfilled and, to some extent even exceeded. The strategies to assemble the structures on the *small scale* can be divided into two classes: top-down and bottom-up as depicted in Figure 1.1. The former strategy typically utilizes lithographic techniques in which a beam of e.g. electrons is scanned in a predetermined pattern over a surface that has been coated with an electron-sensitive resist film. Once the exposed or non-exposed areas are chemically removed, a mask forms that serves as a platform for miniaturized electronics. The smallest feature size depends strongly on the used wavelength and currently, dimensions just below 100 nanometres can be reached with photolithography. Smaller wavelength X-ray and electron beam lithographies can provide patterns down to about 10 nanometres but they are impractical in an industrial setting. Top-down strategy includes also e.g. nanoimprinting and stamping techniques where a pattern is transferred onto a surface by mechanically stamping with a master that has been prepared using high-resolution techniques such as electron or X-ray beam lithography. Features down to 10 nm have been demonstrated in nanoimprint lithography[1] and the technique holds a promise but is still in the research stage. Though effective at the microscale, all top-down techniques suffer common drawbacks: It becomes increasingly difficult and expensive to utilize them at the nanoscale and additionally arbitrary three-dimensional patterns are difficult to obtain by using the above-mentioned planar techniques.

On the other hand, why not let the molecules do all the work? If a right set of molecules are placed in a suitable environment, the molecules will as-

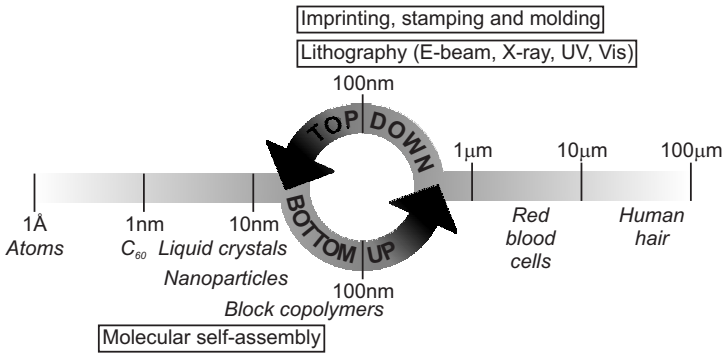

Figure 1.1. Bottom-up and top-down strategies to assemble structures on the nanoscale can be combined to achieve control - both at the molecular level and macroscopic dimensions.

semble themselves into sophisticated architectures at the molecular level. This bottom-up strategy of molecular self-assembly utilizes the energetically favorable weak physical interactions[†] that interconnect the molecules, to control and direct the assembly from molecular level to macroscopic scale.[2] Inspiration for the approach is found in nature where basically everything starting from the formation of the famous DNA double helix, is governed by physical interactions. Recently, several efforts have been made to combine the two strategies (Fig. 1.1) by using self-assembly to generate the nanoscale features and traditional microelectronics processes to construct the nanoscale elements.[3] Even though at some point it will become cost-effective to employ the bottom-up self-assembly in ever-increasing miniaturization, the potential of self-assembly is not in small size but in complex organization and collective operation.[2] Moreover, self-assembly is the only feasible method for creating a diverse set of nanostructures and nano-objects. Ensuring that the molecules assemble correctly is, however, difficult and due to the weak physical interactions, the formed structures are typically only local and contain large amount of defects.

1.1 An outline of the thesis

In this thesis we strive to explore feasible ways, on one hand, to control the formation of nanoscale polymeric structures and, on the other hand, to align the locally ordered structures to macroscopic dimensions in order to obtain anisotropic materials and functions.

In Chapter 2, we show the first example of how charge-transfer complexation between C_{60} fullerenes and electron-donating units of block copolymers can be used to control and direct the self-assembly of fullerene based materials. The alignment of randomly oriented domains of nanostructured material over macroscopic length scales is the topic of Chapter 3. We present details of a rheo-optical instrument design that we have constructed to shine light on the alignment dynamics of soft matter. Alignment of randomly oriented domains is not only useful for obtaining macroscopically anisotropic materials and functions, but it can also be a prerequisite for characterization of the local structures. This aspect is demonstrated for liquid crystalline (LC) diblock copolymers which, upon inducing flow alignment, are shown to exhibit coexistence of two orthogonal orientations of the LC phase within the copolymer lamellae. Furthermore, we demonstrate that ionic complexes forming a columnar LC phase can be efficiently aligned within polymer blends upon shearing, taken that the matrix polymers have sufficiently high molecular weight. This concept allows a simple route for macroscopically aligned nanocomposites with conjugated columnar LC functional additives. Finally, in Chapter 4, control of nanoscale morphology in polymer/fullerene nanocomposite thin film devices is shown to allow tuning of the electrical switching which can enable construction of a memory unit. The working principles of such thin film organic memory devices have remained debated and the first systematic approach is here undertaken to tailor the active material composition and to study the morphology vs. functionality relationship.

[†]Donor-acceptor, ionic, π-π and metal coordination interactions as well as hydrogen bonds and van der Waals forces.

Publication I

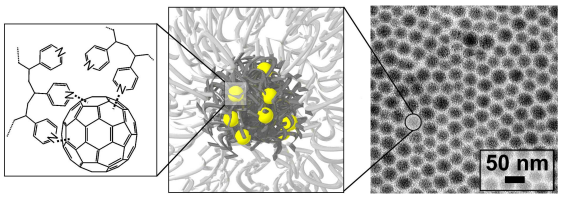

2 Assembly of Small Molecules in Block Copolymer Domains

2.1 Block Copolymer Self-Assembly

Block copolymers are well-known to self-assemble into a large variety of microphase separated superlattices with characteristic dimensions in the range 10-100 nm.[4–8] The formed nanoscale structure depends on the molecular weight, segment size, strength of the interaction between the constituent blocks and the composition of the copolymer i.e. the volume fraction of one of the blocks.[9] For AB diblocks, in addition to the classical morphologies shown in Figure 2.1, bicontinuous gyroid morphology is known to be stable as confirmed by both theory[10] and experiment.[4, 11]

More recently, several efforts have been made to combine block copolymer self-assembly with nanoparticles to design materials that possess desirable properties of the two components. The nanoparticles often aggregate to larger clusters which diminishes the benefits of the nanoscopic dimension. The assembly of the nanoparticles within the block copolymer domains can, however, be controlled and directed by careful selection of the ligands that are attached to the surface of the nanoparticles and interact with the polymer. It has been shown that, in addition to being plain scaffolds to nanoparticles,[12–14] block copolymers can have a much more complex interplay with the nanoparticles leading to alteration of both the orientation[15–17] and the morphology[18–24] of the copolymer domains.

Even though research on block copolymer self-assembly to control the aggregation, size and arrangement of inorganic nanoparticles has been particularly active during the past five years,[25] research on their organic counterparts e.g. fullerenes [26] has been very limited despite their wide range of applications.

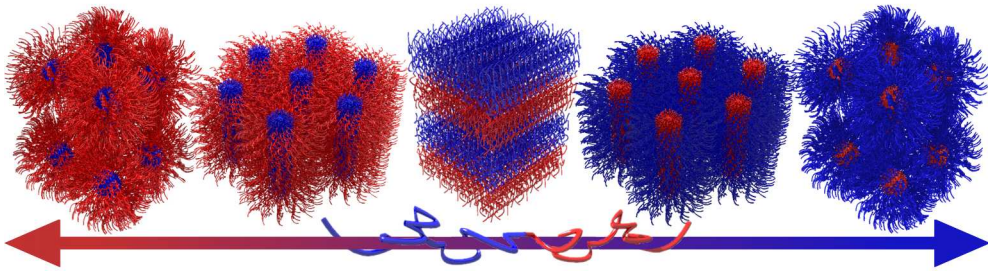

Figure 2.1. Schematic of the classical body-centred cubic, hexagonal-packed cylinder, and lamellar morphologies of diblock copolymers.

2.2 Pushing and pulling polymers around fullerenes

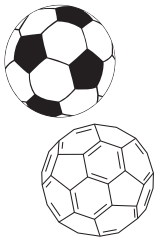

Figure 2.2. C_{60} resembles a football one nanometre in diameter.

Fullerenes are hollow spherical, ellipsoidal or tubular cage-like carbon molecules that constitute a class of carbon allotropes. The first experimental observation of fullerenes was made in 1985 by Harold Kroto, James Heath, Yuan Liu, Sean O'Brien, Robert Curl and Richard Smalley when they found evidence that a C_{60} molecule self-assembled spontaneously in a hot nucleating carbon plasma.[27] The discovery of the fullerenes is one remarkable example of scientific breakthrough,[28] although unbeknown to the discoverers at that time, essential theoretical work preceded the discovery.[29–31] The C_{60} molecule consists of 60 carbon atoms that are arranged into a roughly spherical cage with 32 faces, 12 of which are pentagonal and 20 hexagonal. Similar objects are commonly encountered as footballs (see Fig. 2.2) or architectural structures and it was this connection that inspired the discoverers as they named the molecule *Buckminsterfullerene* after an architect Richard Buckminster Fuller whose geodesic dome the molecule resembles.[†] The field of fullerene science finally exploded after Krätschmer *et al.* succeeded in extracting macroscopic quantities of C_{60} and led the way in the bulk production of the fullerenes.[32–35] The fascinating electronic, magnetic and physicochemical properties of C_{60} arise from its closed-shell configuration that consists of 30 bonding molecular orbitals with 60 p electrons.[36, 37] The high degree of symmetry in the arrangement of the molecular orbitals has provided the basis for the intriguing optical,[38, 39] semiconducting,[40] conducting,[41] superconducting[42, 43] and magnetic[44–47] behavior of the underivatized C_{60}. However, the potential applications are often limited due to the difficult processability of the fullerenes. To be more precise, C_{60} is usually insoluble or in the best case sparingly soluble to most known solvents and due to its high aggregation tendency it becomes even less soluble.[48] Various fullerene derivatives have been synthesized to overcome this obstacle.[49–56] Another approach that has turned out to be particularly feasible is to utilize the ease of processing of polymers. The simplest way to combine polymers with fullerenes, is to mix the two components in a common solvent and then remove the solvent via evaporation. Better control of the final product is often achieved by using covalent bonds to chemically connect the fullerenes to the polymers and this can be done in several different ways: through reaction between the fullerenes and the polymer during the polymerization,[57–59] through favorable reaction between a preformed polymer and the fullerenes,[60–62] through polymerization of a fullerene containing monomer[63, 64] or by growing a dendrimer from the fullerene[65, 66]. In further effort to improve the solubility, to control the assembly and aggregation and also to provide further functionalities to fullerene-based materials, fullerenes have been combined with block copolymer self-assembly.[67–72] In addition to covalent interactions,[73–75] complementary physical interactions, e.g. acid-base[76] and hydrogen bonding[26] have been used to connect the fullerenes to specific chemical groups of block copolymers. Because fullerenes are known to form noncovalent donor-acceptor complexes with

[†]Other alternatives had similar connection: ballene, spherene, soccerene, carbosoccer, ...

various low molecular mass species,[77–83] a question arises as to whether charge-transfer interaction can also be used to connect the fullerenes to block copolymers.

In Publication **I** we answer to this question and describe a particularly facile method for controlled self-assembly of underivatized fullerenes in block copolymer domains via formation of charge-transfer complexes between the electron-accepting C_{60} molecules and electron-donating moieties of poly(styrene-*block*-4-vinylpyridine), PS-P4VP (Fig. 2.3(a)). Let us first discuss the solution properties of C_{60} mixtures. The ultraviolet-visible (UV-Vis) spectrum of C_{60} in xylene shows a broad and only weakly structured absorption band as shown in Figure 2.3(b). If pyridine is used as a solvent instead of xylene, the spectrum initially resembles that of C_{60} dissolved in xylene (Fig. 2.3(c)). Upon aging, however, the color of the C_{60}/pyridine solution changes from purple to brown, which manifests in the UV-vis spectra as an increase in the absorbance in the region 450-550 nm (Fig. 2.3(c)). Such an observation agrees with the formation of charge-transfer complexes between the electron-donating pyridine solvent and the electron-accepting fullerenes.[77–79, 83] A binary mixture of C_{60}/xylene and a ternary mixture consisting of PS/C_{60} in xylene show roughly similar absorption spectra, and they do not change notably even during an aging time of 8 months (Fig. 2.3(b)). However, the situation is different if PS-P4VP/C_{60} is dissolved in xylene. The freshly prepared micellar PS-P4VP/C_{60} block copolymer solution is purple, and its absorption spectrum is qualitatively similar to that of PS/C_{60} in xylene (Fig. 2.3(c)).

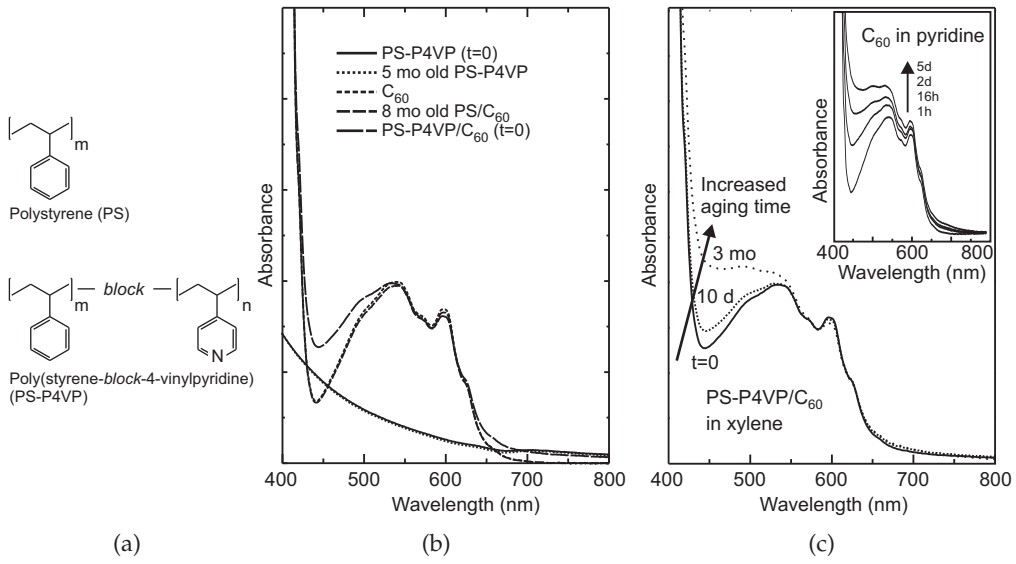

Figure 2.3. (a) Polystyrene (PS) and poly(styrene-*block*-4-vinylpyridine) (PS-P4VP). (b) UV-Vis spectra of PS-P4VP, C_{60}, PS/C_{60} and PS-P4VP/C_{60} dissolved in xylene. (c) UV-vis spectra at different aging times for PS-P4VP/ C_{60} dissolved in xylene. The spectra are shown for a freshly prepared purple solution as well as for the aging times of 10 days and 3 months, leading to brown solutions. The inset shows the spectra for C_{60} dissolved in pyridine solvent. The aging times in this case are 1 h, 16 h, 2 days, and 5 days. Reproduced with permission from Publication **I**. ©2006 American Chemical Society.

Upon aging, however, the absorbance in the region ca. 450-550 nm increases, and the solution becomes brown, similar to the solutions of C_{60} in pyridine. The increased absorbance and color change in aged PS-P4VP/C_{60} xylene solutions can therefore be explained based on charge-transfer complexation between C_{60} and the pyridine units of the block copolymer which is also supported by infrared spectroscopy.

Next, bulk and thin film samples were prepared from the PS-P4VP/C_{60} mixtures. An unexpected morphological change from cylinders (prepared from *fresh* xylene solutions) to spheres (prepared from *aged* xylene solutions) was observed both in bulk and thin films (Fig. 2.4) as evidenced by transmission electron microscopy (TEM) and small angle X-ray scattering (SAXS). The morphologi-

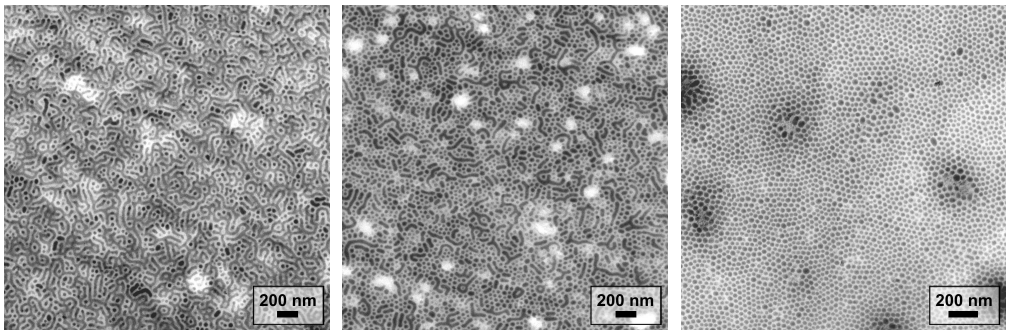

(a) (b) (c)

Figure 2.4. Transmission electron micrographs of thin films: (a) pure PS-P4VP, (b) PS-P4VP/C_{60} prepared from a fresh purple xylene solution, and (c) PS-P4VP/C_{60} prepared from an aged 3 months old brown xylene solution. The P4VP domains appear dark due to I_2 stain. Reproduced with permission from Publication **I**. ©2006 American Chemical Society.

cal change is unexpected because according to block copolymer theories,[4] selective incorporation of small molecular species or nanoparticles within the minority block of hexagonally self-assembled cylindrical diblock copolymer system should render the morphology toward lamellar structures. This feature can be depicted with Figure 2.1 where the initial state is the second morphology from the left.[†] If the volume fraction of the blue P4VP domain increases due to e.g. selective addition of small molecules, the change in the morphology should be toward the blue arrow and lamellar morphology and not toward the red arrow and spherical P4VP morphology as was observed. However, this discrepancy can be explained by the formation of the charge-transfer complexes between the C_{60} molecules and pyridines in the core of PS-P4VP micelles (Fig. 2.5). In freshly prepared xylene solutions (< 2 wt%) the block copolymer forms spherical micelles with PS corona and P4VP cores because xylene is a poor solvent for P4VP, and it is thus expelled from the xylene. As a result the C_{60} molecules are more likely to be found in the PS domains and not in the P4VP micellar cores. Accordingly, thin films or bulk samples prepared from the fresh solutions, show swelling of the PS domains. However, upon aging, the UV-Vis and infrared spectroscopy showed interaction between the pyridines of the PS-P4VP and the C_{60}

[†]The blue and red chains refer to P4VP and PS chains, respectively

molecules. This suggests that, with time, part of the C_{60} molecules penetrate into the P4VP cores of the PS-P4VP micelles and form charge-transfer complexes with the pyridines (see Fig. 2.5). As C_{60} can accept up to six electrons[84, 85] and thus interact simultaneously with up to six pyridine groups, the C_{60} molecules can bind several P4VP chains together via charge-transfer interaction. Such multiple interactions combined with the strong tendency of C_{60} molecules to aggregate render the morphology toward spherical structures even though the volume fraction of P4VP domain increases and the theories[4] suggest a change toward lamellar morphology.

Related morphological change but due to different types of interactions and materials has been reported in polystyrene-*block*-poly(ethylene oxide) (PS-PEO) block copolymer thin films upon addition of cadmium sulfide (CdS) nanoparticles.[86] The morphological change from PEO cylinders to CdS/PEO spheres was explained by the presence of multiple hydrogen bonds between surface-hydrox-

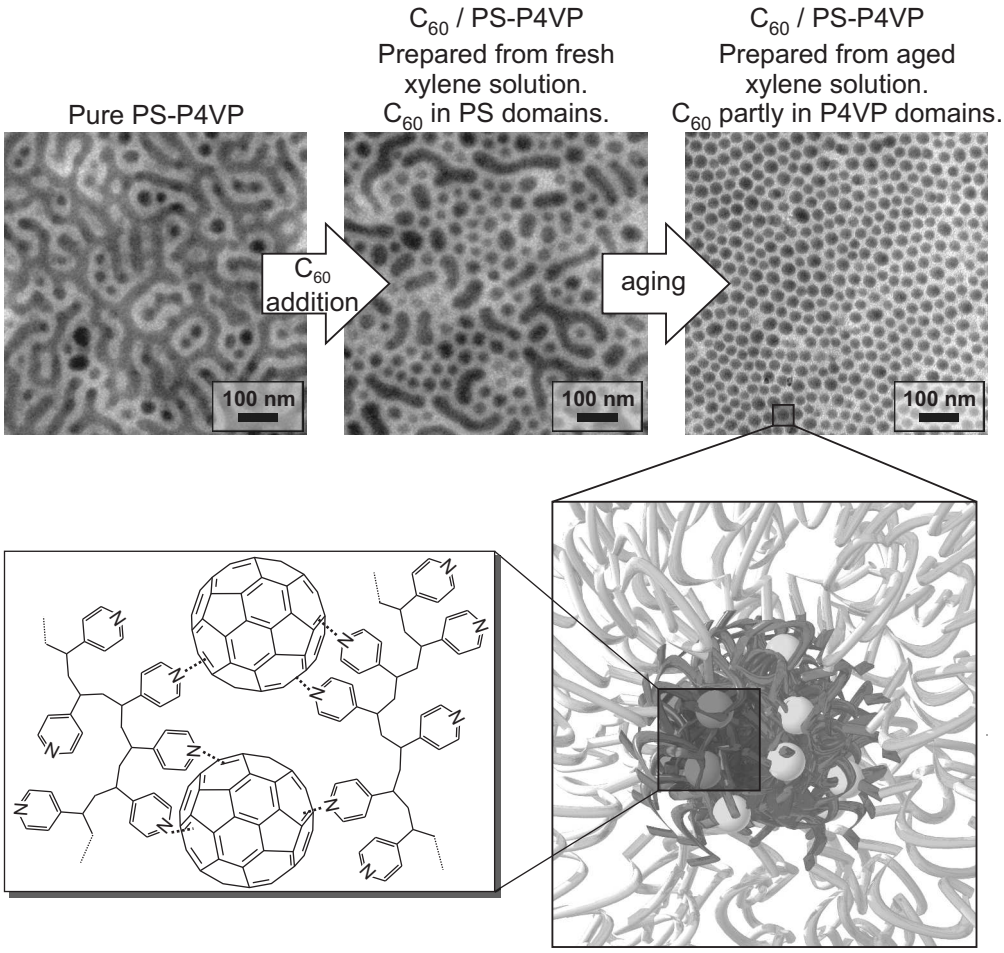

Figure 2.5. Schematic representation of the self-assembled PS-P4VP/C_{60} structures formed through charge-transfer complexation. The strong tendency of C_{60} molecules to aggregate combined with the possibility that each C_{60} molecule can bind multiple P4VP chains together through charge-transfer interarction is suggested to cause the morphological change from P4VP cylinders to C_{60}-containing P4VP spheres. Reproduced with permission from Publication **I**. ©2006 American Chemical Society.

ylated CdS nanoparticles and PEO. Furthermore, Fujita *et al.* reported spherical morphologies of PS-P4VP micelles in the presence of carboxylic acid-functionalized C_{60} molecules.[26] An explanation was suggested that the underlying mechanism could be due to the formation of hydrogen bonds between pyridine and C_{60}-COOH. However, our present work suggests that charge-transfer interaction may have played a role also in their work, in particular as they reported a similar color change to brown that was also observed in our aged PS-P4VP/C_{60} xylene solutions. Additionally, we have demonstrated that underivatized C_{60} without additional functional groups is able to interact with block copolymers and can control the self-assembly via charge-transfer complexation.

Publications II, III and IV

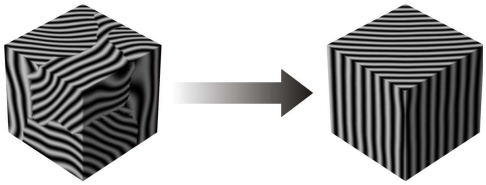

3 From local to global order

3.1 Background

Molecular self-assembly typically leads to locally ordered domains with a large number of defects in the local structure. The local randomly oriented domains often lack mutual alignment and therefore the material remains macroscopically disordered and isotropic which limits potential applications in the fields of electronics and optics in particular. The objective is to extend the local structures to macroscale and, quite often, also to control the orientation of the domains. As an example, in filtering and separation applications, control of the orientation of small pores that travel through the membrane is required whereas control of the exact position of an individual pore is not needed.[87, 88] On the other hand, for position sensitive applications such as memory devices, control of both orientation and long range order are often required.[3, 89] Spatial restrictions in confined systems e.g. in thin films may already as such enable control of ordered structures over macroscopic dimensions. Spin coating a thin film from a block copolymer solution will lead to randomly oriented small domains but upon thermal or solvent annealing of the films the domain size can drastically increase due to decrease in the amount of energetically costly grain boundaries and defects.[90–95]

The local anisotropic domains can be aligned over macroscopic length scales and the number of defects can be considerably reduced through post-processing by using e.g. graphoepitaxy,[90, 96] electric,[97–100] magnetic[101–104] or flow fields. In graphoepitaxy, predefined surface relief patterns are used to bias the epitaxial growth and orientation of the microdomains of block copolymer thin films.[90] The alignment of block copolymers under an influence of an electric field has been explained based on the difference between the dielectric constants of the constituent blocks. The dielectric breakdown of the material, however, limits the maximum field strength that can be used for the alignment, especially in thin films. In terms of magnetic fields, it is the spatial variation of the magnetic permeability of the constituent blocks that determines the free energy of the system under magnetic field and directs the alignment of the microdomains similarly as variation in the dielectric constant does in the case of the electric field. Use of a magnetic field for alignment purposes has one advantage over using an electric field, namely, the risk of dielectric breakdown is not as probable. The reported values for the strength of the magnetic field to align a block copolymer system are typically in the range of 1-10 T and this requirement undoubtedly leads to technological limitations.[101–104] Furthermore, all the systems that have been reported to date contain crystalline or liquid crystalline moieties that are responsible for the

alignment whereas there are no reports on the alignment of simple amorphous-amorphous block copolymers by using magnetic fields. The analogy between the magnetic and electric fields, nevertheless, suggests that similar alignment by using either magnetic or electric field should be possible in completely amorphous systems as well.

3.2 Flow-induced alignment

Flow or mechanical deformation is by far the most efficient technique to align block copolymer melts in bulk.[105–131] The possibility of using a flow field to align the copolymer microdomains was first pointed out by Keller and coworkers in extruded rods of poly(styrene-*block*-butadiene-*block*-styrene) (PS-PB-PS).[105] The hexagonally arranged cylinders of PS were found to align parallel to the stretch direction in the extruded rods. Keller and coworkers deduced that the extruded *macroscopic crystals* would have a *pronounced directionality in property* leading to anisotropic elastomers and different mechanical properties.[105] However, rheological conditions could not be easily controlled and monitored in extrusion processes and a significant advancement in this perspective was provided by Hadzioannou and coworkers when they introduced a parallel plate shear device.[107] When a cylindrical structure of poly(styrene-*block*-isoprene-*block*-styrene) (PS-PI-PS) triblock copolymer was subjected to an oscillatory shear flow field in the molten state, Hadziioannou and coworkers observed that the cylinders aligned parallel to the flow direction.[107] Koppi *et al.* introduced another substantial technological improvement which allowed simultaneous small-angle neutron scattering (SANS) experiments under the influence of the flow field.[110–112] The improved shear apparatus led the way for the discovery of a so-called *flipping* phenomenon where the final aligned state of the block copolymer lamellae could be changed from parallel to perpendicular (see Fig. 3.1) by controlling the oscillation frequency and temperature.[110] Control of the orientation of the block copoly-

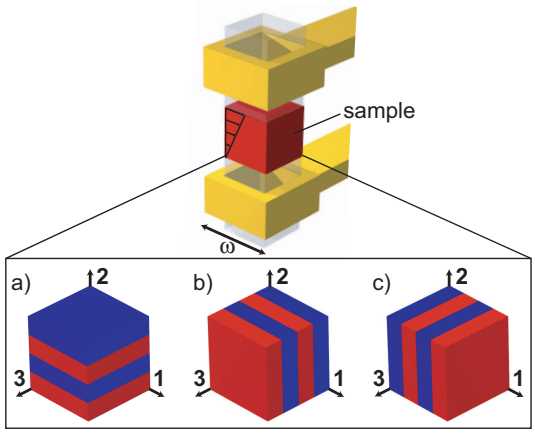

Figure 3.1. Schematic illustration of the possible shear-induced macroscale orientations of lamellar block copolymer system, namely a) parallel; b) perpendicular and c) transverse orientation. Reprinted with permission from **II**. ©2007 American Institute of Physics.

mer lamellae offers a feasible means to obtain macroscopically different materials from the same polymer by simply tuning the processing conditions. This discovery finally opened the floodgates for research on block copolymer melt dynamics and to date, all block copolymer morphologies have been subjected to extensional or shear flow field and their flow behavior has been studied as a function of various processing parameters.

The final aligned state of a lamellar block copolymer is governed mainly by four critical processing parameters:[132]

i) shear rate, $\dot{\gamma}$

ii) strain amplitude, γ_0

iii) temperature with respect to order-disorder transition temperature

iv) the initial morphological state of the sample.

Powerful material characterization techniques are required to clarify which type of flow best induces macroscale order and which processing parameters determine the direction, perfection and rate of the alignment for a particular copolymer system. These techniques can be divided into two groups: those that are performed *in-situ* during shear deformation and those that are applicable only after alignment (*ex-situ*) and involve additional processing. *In-situ* SAXS[125, 133–135] and SANS[109–112, 136] can be used to follow the alignment dynamics in detail without disturbing the sample under shear. Rheo-optics[115–117, 119, 137, 138] is especially applicable to follow fast alignment processes but it cannot provide detailed structural information unlike the scattering techniques. Viscoelastic response of the aligned sample[121, 127] or analysis of the higher harmonics in the torque response[139, 140] can also be used to follow the alignment dynamics but most probably due to the non-trivial connection between the viscoelastic response and the final aligned state, they have remained less popular. Unfortunately, no one technique alone is adequate for providing all of the necessary structural information. For instance, *in-situ* scattering techniques suffer from relatively poor time resolution and must typically be conducted in large-scale e.g. neutron or synchrotron radiation facilities to obtain high enough intensity. Even so, scattering measurements can be performed simultaneously in only one direction which limits drawing conclusions on the three-dimensional structure. Kornfield and coworkers have shown that combination of the real-time rheo-optical methods with the more detailed *ex-situ* structural characterization techniques (SAXS, SANS and/or TEM) can provide a powerful technique to elucidate the alignment dynamics of lamellar block copolymer systems in particular.[115, 116, 138]

3.3 Rheo-optics as a tool to follow the pathways to macroscale order

Birefringence of lamellar block copolymer melts can be used to follow the direction, rate and degree of alignment under shear.[115] This variable has two distinct contributions which arise from the anisotropy in the polymer monomer (intrinsic birefringence Δn_i) and block copolymer microstructure (form birefringence

Δn_f). Even though the latter contribution is related to larger length scales and thus follows the overall alignment dynamics better, rheo-optics has been successfully applied to systems where the refractive indices of the constituent blocks are either significantly different[117] ($\Delta n_f >> \Delta n_i$) or nearly equal[137] ($\Delta n_i >> \Delta n_f$).

Experimental setup

In Publication **II** we introduce a rheo-optical setup where the dynamic birefringence is measured by utilizing polarization modulation technique (Fig. 3.2).

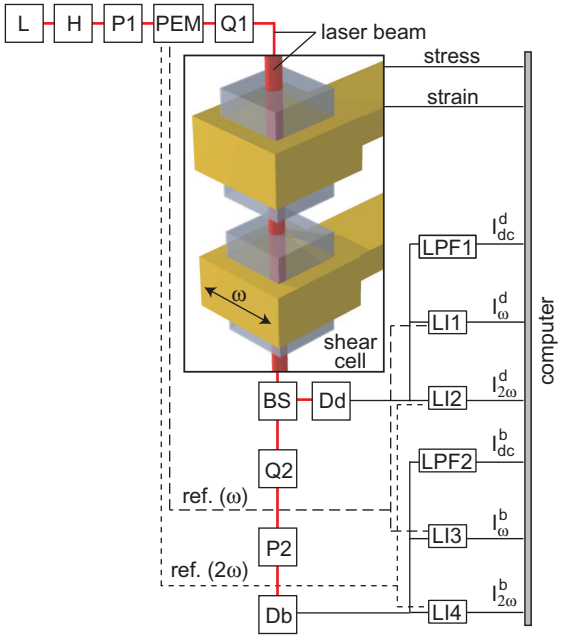

Figure 3.2. Schematic illustration of the apparatus: (L) laser; (H) half-wave plate; (P) polarizer; (PEM) photoelastic modulator; (Q) quarter-wave plate; sample in the shear cell; (BS) beamsplitter; (Dd) detector for dichroism path; (Db) detector for birefringence path; (LPF) low-pass filter; (LI) lock-in amplifier. Reprinted with permission from **II**. ©2007 American Institute of Physics.

The sample is subjected to an oscillatory shear flow field by placing the sample pellet between two quartz teeth the lower of which is set into oscillatory motion and the upper of which senses the torque that is applied to the sample. After polarization modulation by a photoelastic modulator (PEM), a light beam is directed through the quartz teeth and the sample in between. If the sample is birefringent, the light beam will undergo retardation which is then converted to change in the light intensity by using the optical components following the flow cell and the associated electronics. Besides being birefringent, materials can also be dichroic which means that light is absorbed differently depending on the rotation and polarization state of the incoming light. The instrument can be used to measure low level linear birefringence and/or dichroism as well as their orientation angles and next we will discuss the optics, electronics and mechanics of the experimental setup.

Let us begin with the fundamentals of polarized light and its interaction with anisotropic media. A pure x- and y-plane polarized light with an amplitude E_0

and wavelength λ can be expressed as follows:

$$\boldsymbol{E}_x(z,t) = E_0 \cos k(z-\omega t)\hat{\boldsymbol{x}} \tag{3.1}$$

$$\boldsymbol{E}_y(z,t) = E_0 \cos[k(z-\omega t)-\phi]\hat{\boldsymbol{y}}, \tag{3.2}$$

where $\hat{\boldsymbol{x}}$, $\hat{\boldsymbol{y}}$ are unit vectors, ω is the frequency, ϕ is a relative phase angle and the wave vector k is given by $k = 2\pi/\lambda$. The net effect of the x- and y-plane polarized light is simply the sum of equations 3.1 and 3.2 since the light waves obey the superposition principle. This sum depends strongly on ϕ as illustrated in Figure 3.3 which shows a schematic of different polarization states. As an example

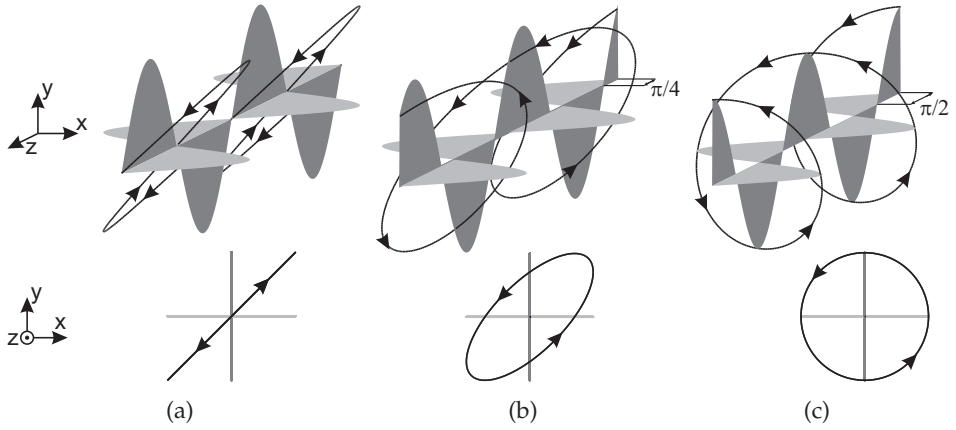

Figure 3.3. Schematic illustration of (a) plane polarization, $\phi = 0$, (b) elliptical polarization, $\phi = \pi/4$ and (c) circular polarization, $\phi = \pi/2$. The light gray and dark gray surfaces depict the x and y components of the polarized light, respectively, and the solid curve is the amplitude of the resultant.

circularly polarized light ($\phi = \pi/2$) can be considered as a sum of two orthogonal linearly polarized waves with equal amplitudes which are $\phi = \pi/2$ out of phase with each other (Fig. 3.3(c)). In practice such a circularly polarized light can be obtained from unpolarized monochromatic light by using a linear polarizer and an optical element called quarter-wave plate or retarder. After passing through the linear polarizer the light beam is directed through the quarter-wave plate at 45° angle between the polarization plane of the light beam and the fast and slow axis of the wave plate. The polarized light beam can now be divided into two orthogonal parts: the x-axis (slow) and y-axis (fast) component. As the light beam passes through the quarter-wave plate, the former component is retarded by $\delta = \pi/2$ rad or one-quarter of a wave ($\lambda/4$) and the resultant beam becomes circularly polarized as illustrated in Figure 3.3(c). The quantity δ is called the retardance and it is related to birefringence Δn by

$$\delta = \frac{2\pi n_1 d}{\lambda} - \frac{2\pi n_3 d}{\lambda} = \frac{2\pi \Delta n_{13} d}{\lambda}, \tag{3.3}$$

where n_1 and n_3 are the refractive indices of the material along two orthogonal axis 1 and 3 (Fig. 3.1), λ is the wavelength and d is the thickness of the material. In rheo-optics or birefringence measurements in general it is the retardance, δ that is being measured.

The analysis of the optical trains consisting of various polarizing elements and anisotropic media can be carried out in a straightforward manner by using Mueller calculus.[141, 142] An optical component or anisotropic sample is described with a Mueller matrix $\boldsymbol{M} \in \mathbb{R}^{4\times4}$ whereas a Stokes vector $\boldsymbol{S} \in \mathbb{R}^4$ is used to represent the polarization state of the light beam. As an example, a sample that exhibits linear and circular dichroism and birefringence can be expressed in the limit of small anisotropies via the following Mueller matrix

$$\boldsymbol{M}_S = \begin{bmatrix} 1 & -\delta'' \cos(2\theta'') & -\delta'' \sin(2\theta'') & \delta''_c \\ -\delta'' \cos(2\theta'') & 1 & \delta'_c & -\delta' \sin(2\theta') \\ -\delta'' \sin(2\theta'') & -\delta'_c & 1 & \delta' \cos(2\theta') \\ \delta''_c & \delta' \sin(2\theta') & -\delta' \cos(2\theta') & 1 \end{bmatrix}, \tag{3.4}$$

where δ' and θ' are the linear retardation and its orientation angle, δ'' and θ'' are linear extinction and its orientation angle, δ'_c and δ''_c are circular retardation and extinction, respectively. The polarization state of the incoming light beam before ($\boldsymbol{S}_0$) and after ($\boldsymbol{S}_1$) it has passed through all the optical components and the sample can be written using the following Stokes vectors

$$\boldsymbol{S}_1 = \boldsymbol{M}_{PSA} \boldsymbol{M}_S \boldsymbol{M}_{PSG} \boldsymbol{S}_0, \tag{3.5}$$

where $\boldsymbol{M}_{PSG}$[†] and $\boldsymbol{M}_{PSA}$[‡] are the products of Mueller matrices of the optical components that are placed before and after the sample, respectively. The first element of the Stokes vector gives the intensity of the light beam ($\boldsymbol{S}_1(1) = I$) and it has two different expressions depending on the branch of the optical train, namely dichroism (D_d) or birefringence (D_b) (Fig. 3.2)

$$\begin{aligned} I_{D_d} &= \boldsymbol{S}^T_{PSA_d} \boldsymbol{M}_S \boldsymbol{S}_{PSG} = \frac{I_1}{2}[1 - \delta'' J_0(\Delta_0)\cos(2\theta'') \\ &\quad -2\delta'' J_1(\Delta_0)\sin(2\theta'')\sin(\omega t) \\ &\quad -2\delta'' J_2(\Delta_0)\cos(2\theta'')\cos(2\omega t)] \qquad (3.6) \\ &= \frac{I_1}{2}[I^d_{DC} + I^d_\omega \sin(\omega t) + I^d_{2\omega}\cos(2\omega t)] \qquad (3.7) \\ I_{D_b} &= \boldsymbol{S}^T_{PSA_b} \boldsymbol{M}_S \boldsymbol{S}_{PSG} = \frac{I_1}{4}[1 - \delta''_c - J_0(\Delta_0)(\delta'' \cos(2\theta'') + \delta' \sin(2\theta')) \\ &\quad -2J_1(\Delta_0)(\delta'' \sin(2\theta'') - \delta' \cos(2\theta'))\sin(\omega t) \\ &\quad -2J_2(\Delta_0)(\delta'' \cos(2\theta'') + \delta' \sin(2\theta'))\cos(2\omega t)] \qquad (3.8) \\ &= \frac{I_1}{4}[I^b_{DC} + I^b_\omega \sin(\omega t) + I^b_{2\omega}\cos(2\omega t)] \qquad (3.9) \end{aligned}$$

where $J_k(x)$, $k = 0, 1, 2$ are Bessel functions of the first kind, ω is PEM's modulation frequency and Δ_0 is PEM's retardation amplitude, $\Delta = \Delta_0 \sin(\omega t)$. Δ_0 can be chosen so that $I^{b/d}_{DC}$ terms in Equations 3.7 and 3.9 become independent of δ and θ i.e. $J_0(\Delta_0 = 2.405) = 0$. The DC-terms ($I^{b/d}_{DC}$) can be directly measured by passing the signals from the detectors through low pass filters whereas the first and second harmonics ($I^{b/d}_\omega$ and $I^{b/d}_{2\omega}$) can be measured by using lock-in amplifiers that are referenced to the PEM's modulation frequency. The latter two terms

[†]Polarization State Generator, PSG
[‡]Polarization State Analyzer, PSA.

are further normalized with the DC terms in order to cancel any effects related to the fluctuations in the intensity of the light source. Finally, $I_{DC'}^{b/d}$, $I_{\omega}^{b/d}$ and $I_{2\omega}^{b/d}$ are used to solve δ', θ' and δ'', θ'' by using Equations 3.6 and 3.8. Finally, linear birefringence ($\Delta n'$) and dichroism ($\Delta n''$) can be obtained from δ' and δ'' by using Equation 3.3. To perform the signal processing and the above mentioned calculations, a measurement program was written with LabVIEW software (National Instruments).

Alignment of a lamellar diblock: A rheo-optical study

To test the performance of the experimental setup, we studied the flow alignment dynamics of a well-known lamellar diblock copolymer system comprising of poly(styrene-*block*-isoprene) (PS-PI, see Fig. 3.4(a)). Based on SAXS, the diblock copolymer was known to self-assemble into a lamellar morphology with a d-spacing of 22 nm. The birefringence of PS-PI is dominated by the form birefringence[143, 144] and therefore Δn_{13} is directly related to the orientation distribution of the lamellae.[119] As an example, a perfectly aligned parallel state (Fig. 3.1) would give zero birefringence whereas perpendicular or transverse orientation would lead to a non-zero value $|\Delta n_{13}| > 0$.

The diblock copolymer sample was subjected to large amplitude oscillatory shear flow at two different working temperatures, namely 115 °C and 145 °C and the evolution of the dynamic moduli and birefringence under shear were monitored *in situ* (Fig. 3.4). Both moduli show a fast initial drop which is followed by a slower gradual decay typical for diblock copolymers undergoing a transition from randomly oriented local domains toward macroscopically aligned state. Additionally, Figure 3.4(b) shows that birefringence follows two distinct trajectories depending on the processing temperature. When the diblock copolymer is subjected to shear at 115 °C, birefringence shows a fast initial increase followed by a slower decay. At 145 °C, on the other hand, birefringence first increases rapidly and then gradually flattens. Kornfield and coworkers have extensively

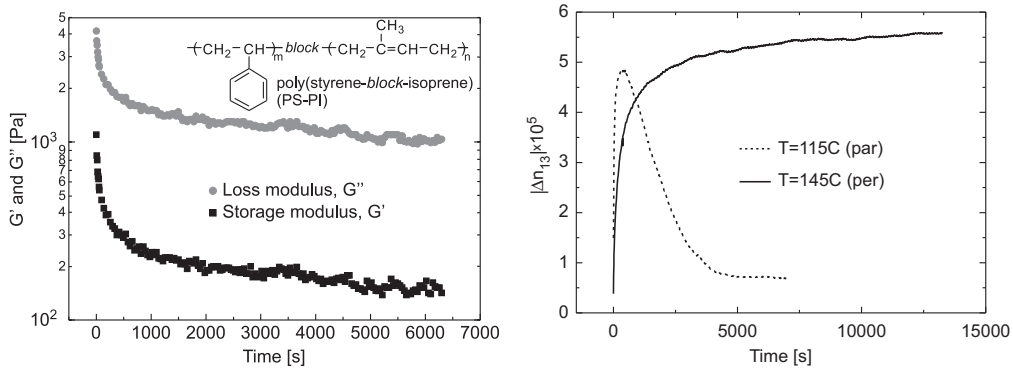

(a) (b)

Figure 3.4. (a) Evolution of the dynamic storage G' and loss modulus G'' of PS-PI during oscillatory shear at 115°C. Oscillation frequency $\omega = 1$ rad/s, shear strain amplitude $\gamma_0 = 0.42$. (b) Evolution of the birefringence during shear alignment. Reprinted with permission from **II**. ©2007 American Institute of Physics.

studied the flow alignment dynamics of PS-PI by using rheo-optical approach. By comparing the different trajectories observed in this study and reported by Kornfield and coworkers[115–117, 138] we can notice that the curve obtained at 115 °C (Fig. 3.4(b)) resembles the route to perpendicular orientation and at 145 °C (Fig. 3.4(b)) the route to parallel orientation. However, more detailed structural characterization is required to verify these conclusions.

After finishing the alignment process, the samples were cooled down to room temperature and removed from the rheometer for more detailed *ex-situ* analysis. Two-dimensional SAXS patterns together with the corresponding azimuthal scans are shown in Figure 3.5. The scattering patterns support the conclusions drawn from the trajectories of the birefringence, i.e. at lower temperature (115 °C) the material progresses toward parallel and at higher temperature (145 °C) toward perpendicular orientation.

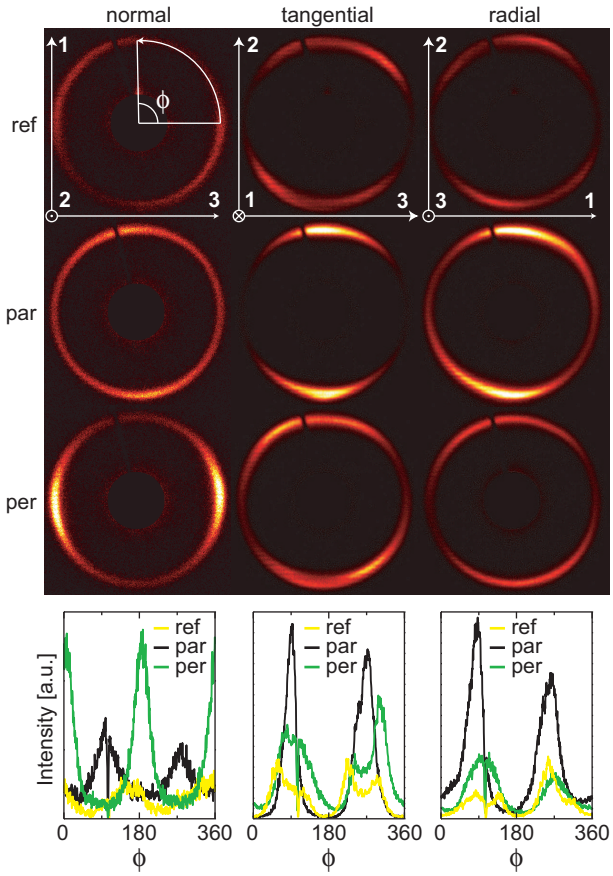

Figure 3.5. Two-dimensional SAXS patterns of the first order Debye rings in normal, tangential and radial views for (ref) a reference sample and for samples subjected to oscillatory shear flow ($\omega = 1.0$ rad/s, γ_0=42%) at (par) 115°C and (per) 145°C. Azimuthal scans from the first order Debye rings are shown at the bottom of the figure. Reprinted with permission from **II**. ©2007 American Institute of Physics.

3.4 Side chain liquid crystalline block copolymers

Liquid crystalline materials cannot be simply categorized as solid, liquid or gas as they possess mechanical and symmetry properties between those of a liquid and a crystal.[145, 146] Due to this reason they are often said to exhibit intermediate or *mesomorphic phases*. Following the more precise definition by de Gennes, liquid crystals *are systems in which a liquid-like order exists at least in one direction of space and in which some degree of anisotropy is present*.[145] A variety of phases, transitions and phenomena can be observed in liquid crystalline materials depending on external conditions and the type of the molecular building blocks i.e. mesogens of the liquid crystals.[145–148]

The rich diversity of liquid crystalline mesophases can furthermore be combined with block copolymer self-assembly to form various hierarchical structures of e.g. side chain liquid crystalline block copolymers.[149–151] Recently, understanding the interplay between the two structural hierarchies has been of particular scientific interest.[102, 152–154] Lamellar-*within*-lamellar morphologies, where mesogens form smectic layers within block copolymer lamellae, can be obtained for a wide range of volume fractions of the copolymer (Fig. 3.6). The smectic layers typically align perpendicular to the copolymer lamellae (Fig. 3.6(b)) independently of the type of the mesogen (e.g., azobenzene, biphenyl, or cholesteryl).[155–158] However, parallel orientation (Fig. 3.6(c)) has also been observed and was first reported by Hammond and coworkers.[159, 160] They found that diblock copolymers bearing a hexyl spacer between the mesogen and the polymer backbone exhibited perpendicular orientation of the smectic layers whereas copolymers bearing a longer decyl spacer led to parallel orientation in roll-cast films. In melt-drawn fibers, on the contrary, only perpendicular orientation was observed. Hammond and coworkers concluded that the length of the alkyl spacer determines the orientation of the smectic layers due to difference in the decoupling of the mesogens

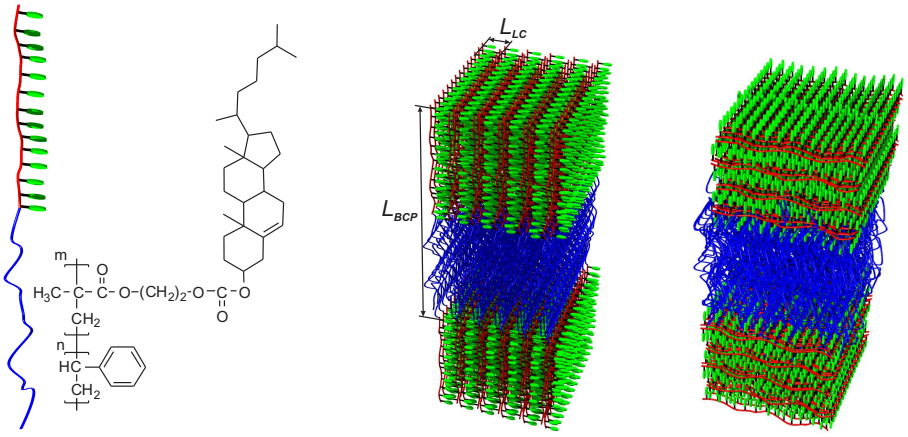

Figure 3.6. (a) Chemical structure and schematic model of the poly(styrene-*block*-2-cholesteryloxycarbonyloxy ethyl methacrylate) i.e. PS-PChEMA diblock copolymer. Schematic representation of (b) perpendicular and (c) parallel orientation of the LC PChEMA subphase. $L_{BCP} = 280$ Å and $L_{LC} = 45$ Å

from the polymer backbone.[160, 161]

In Publication **III** we study the morphology of a side chain liquid crystalline diblock copolymer in which only a short oxycarbonyloxy ethyl spacer couples the mesogenic cholesteryl unit to the polymer backbone (Fig. 3.6(a)). Based on SAXS and TEM the block copolymer is known to self-assemble into a hierarchical lamellar-*within*-lamellar morphology as shown in Figure 3.7. To determine whether the smectic layers align parallel (Fig. 3.6(c)) or perpendicular (Fig. 3.6(b)) to the copolymer lamellae, the local isotropic structures shown in Figure 3.7 should be extended over macroscopic length scales so that the orientation of the smectic layers becomes observable.

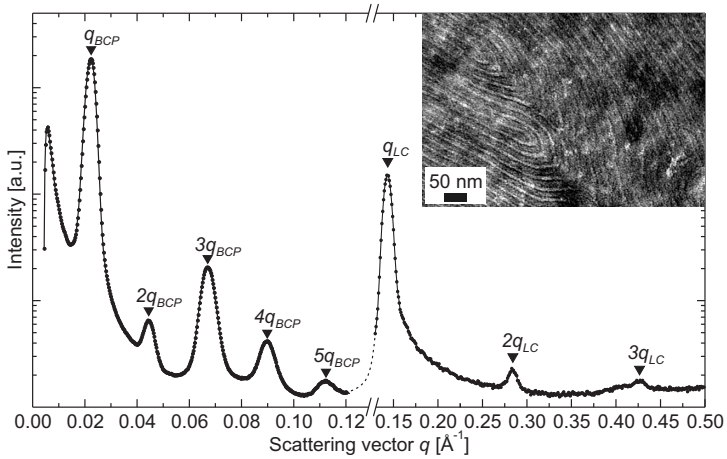

Figure 3.7. Combined SAXS profile of the PS-PChEMA in the low- and high-q region shows five intensity maxima which arise from the lamellar BCP structure (q_{BCP}) and three intensity maxima arising from the LC subphase (q_{LC}). The corresponding TEM micrograph is shown in the inset where PS regions appear darker due to RuO_4 staining.

We used oscillatory shear flow and real-time monitoring by rheo-optics to align the hierarchical structures beyond the local order. The two-dimensional SAXS patterns of the aligned PS-PChEMA pellet recorded in three orthogonal directions are shown as a three-dimensional representation in Figure 3.8b. The lamellar copolymer structure is uniaxially aligned with the lamellae normal pointing along the shear gradient direction as evidenced in the meridional intensity maxima in radial and tangential scattering patterns as well as the low intensity in the isotropic normal scattering pattern (Fig. 3.8b). The smectic layers, on the other hand, have two orthogonal orientations with respect to the uniaxially aligned copolymer lamellae where the normal of the smectic layers is aligned either parallel or perpendicular with respect to the copolymer lamellae normal. This schizophrenic nature of the smectic mesophase is more evident in the azimuthal scans of Figure 3.8c which shows intensity maxima at roughly 180° and 270° arising from the perpendicular and parallel orientation, respectively. The analysis of the azimuthal scans offers a means to estimate the relative occurrence of the different orientations. Numerical integration of the areas corresponding to the parallel and perpendicular orientation in Figure 3.8c gives an estimate that roughly 19 % of the smectic layers are aligned parallel with respect to the copolymer lamellae, the remaining 81 % exhibiting perpendicular orientation. Interest-

ingly, the fraction of the parallel orientation (20 - 35 %) was found to depend on the processing conditions. Increase in either oscillation frequency and/or shear strain amplitude promoted an increase in the relative occurrence of the parallel orientation. Direct imaging with TEM offers another powerful technique to visualize the hierarchical structures[162–164] as shown in Figure 3.8d which confirms the coexistence of the two orthogonal orientations of the smectic layers. The preceding results suggest coexistence of parallel and perpendicular orientations even though on the basis of previous reports[157–161] the smectic layers of PChEMA were expected to align perpendicular to the BCP lamellae. Two questions arise: Why do the parallel and perpendicular orientations coexist? And what is the role of the flow field? Answering these questions is challenging because one should be able to exclude the effect of the flow field and study the orientation of the pristine LC phase but to accomplish this, the material should be well ordered which, on the other hand, requires use of external alignment fields. To overcome these obstacles and to study the material close to thermal equilibrium, a well-aligned sample pellet was further thermally annealed in a high vacuum oven. Upon annealing, the intensity associated with the parallel orientation of the LC phase was

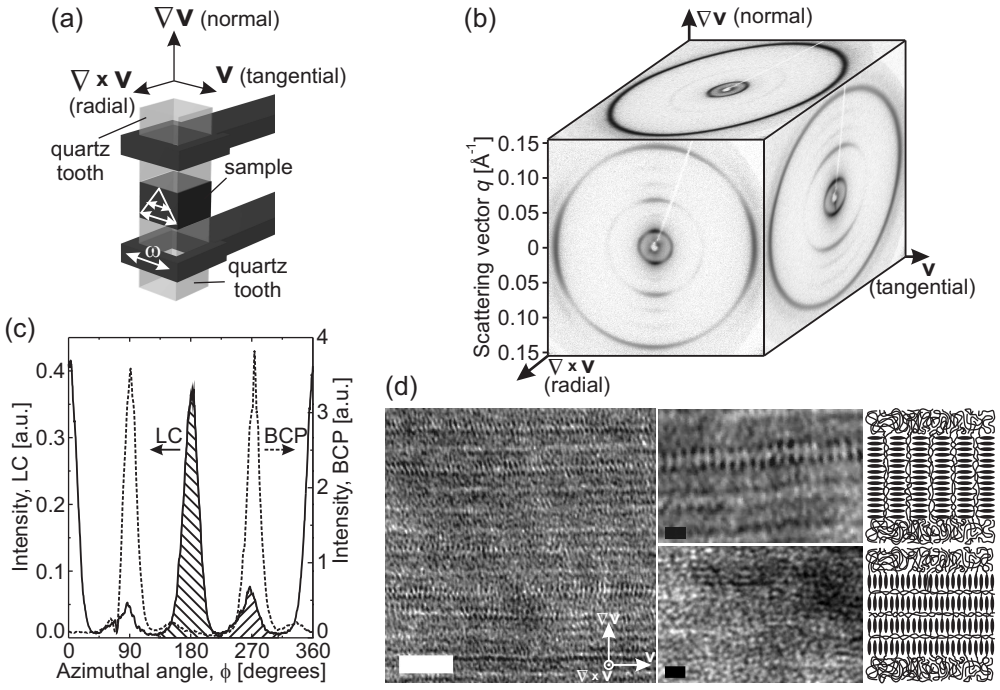

Figure 3.8. (a) Schematic illustration of the flow cell together with the corresponding axis of coordinates. The light beam used for measuring the birefringence travels in the normal direction through the sample and the quartz teeth. (b) SAXS patterns from an aligned sample pellet recorded in normal, tangential and radial direction. (c) Azimuthal scans obtained from the radial SAXS pattern for the first order peaks arising from the liquid crystalline subphase (solid curve, $q_{LC} = 0.1395$ Å^{-1}) and block copolymer structure (dashed curve, $q_{BCP} = 0.0221$ Å^{-1}). (d) TEM micrograph from an aligned sample pellet showing both the block copolymer structure as well as the liquid crystalline structure (white scale bar, 50 nm) and higher magnification TEM micrographs (black scale bars, 10 nm) together with the schematic of perpendicular and parallel orientation of the smectic subphase.

found to decrease slightly whereas that of perpendicular orientation increased. These observations suggest that the distribution between the parallel and perpendicular orientation is a result of the competition between the coupling of the cholesteric mesogens to the methacrylate backbone (perpendicular orientation) and the shear induced alignment (parallel orientation).

3.5 Ionic self-assembled complexes

In the preceding section, we discussed the hierarchical structures formed in side chain liquid crystalline block copolymers in which the mesogens were covalently bound to the polymer chain. An alternative and feasible approach which uses non-covalent physical interactions besides the covalent bonds, is termed supramolecular chemistry.[2] As an example, a simple supramolecular counterpart to the previous case is a diblock copolymer in which the mesogens or amphiphiles are bound to the polymer backbone via non-covalent interactions such as electrostatic,[165–167] coordination,[168] hydrogen bonding[163, 169, 170] or a combination of different physical interactions[162, 171, 172] to form related hierarchical structures. One of the main advantages of using non-covalent interactions over the covalent ones, is that the bonds may be opened and reformed reversibly[2, 172] thus enabling e.g. thermally responsive materials and applications.[162, 169, 173]

The synthetic route of ionic self-assembly (ISA) is a branch of supramolecular chemistry which uses electrostatic interactions to couple various molecular building blocks or tectons together to create diverse nanostructures.[174] The ISA route allows facile combination of various functionalities in a modular fashion by complexing different charged functional moieties with ionic surfactants. The surfactants not only allow tuning of the assembly and packing and introduce plasticization, but can also lead to liquid crystallinity.[174] Perylenes which are important organic electron-accepting semiconducting moieties,[175] have been successfully combined with ionic surfactants to form various ISA complexes and nanoscale structures.[176, 177] The formed structures, however, are only local and alignment of the n-type semiconducting perylene moieties is especially desirable, as perylene derivatives are attractive for supramolecular materials,[175] photovoltaics,[178] molecular electronics,[179] liquid-crystalline materials[176, 177, 180] and optical components.[177] However, alignment of ISA materials has turned out to be surprisingly difficult even though shear-induced alignment has been successfully used to align related self-assembled hydrogen-bonded polymer-amphiphile structures over macroscopic length scales.[181–189] A wide variety of different local ISA structures have been reported[174, 176, 190–203] but despite multiple attempts to achieve common macroscopic alignment beyond the local order, none of the tried methods has turned out to be particularly feasible to align ISA complexes that contain aggregated units with strong π-π interactions.[177, 204] Recently, photo-orientation of charged azobenzene-containing ISA complexes has been shown to lead to macroscopic order.[204, 205] Such alignment strategy is, however, only applicable to materials containing photo-active units and therefore cannot be fully generalized.

In Publication **IV** we introduce a facile scheme that can allow overall alignment of the ionic self-assembled complexes beyond the local polydomain-like

order. The scheme is based on blending the ISA complex with a high molecular weight inert polymer, such as polystyrene, and then aligning the ISA complexes within the polymer matrix by subjecting the blend to shear flow at elevated temperatures. The ISA complex used is a cationic *N,N′*-bis(ethylenetrimethylammonium)-perylenediimide (Pery) bearing an ionically bonded anionic bis(2-ethylhexyl) phosphate (BEHP) surfactant (Fig. 3.9).

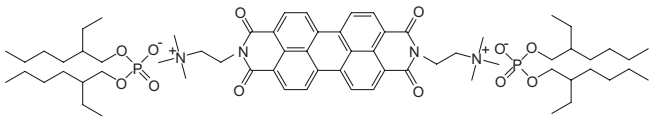

Figure 3.9. N, N'-bis(ethylenetrimethylammonium)-perylenediimide/bis(2- ethylhexyl) phosphate complex, i.e., Pery-BEHP.

The structure of the pure Pery-BEHP complex is first explored by using TEM, SAXS and wide-angle X-ray scattering (WAXS). WAXS results suggest that the planar perylene units exhibit π-stacking with a d-spacing of 3.4 Å (Fig. 3.10(a)). The SAXS pattern, on the other hand, shows several distinct intensity maxima (Fig. 3.10(b)) which can be indexed to a two-dimensional oblique columnar phase, the columns of which constitute of the stacked planar perylene units (Fig. 3.10(d)). This conclusion is also supported by TEM where elongated objects having closely similar d-spacing are observed (Fig. 3.10(c)).

Even if, SAXS and TEM showed well-defined order at the mesoscale, the

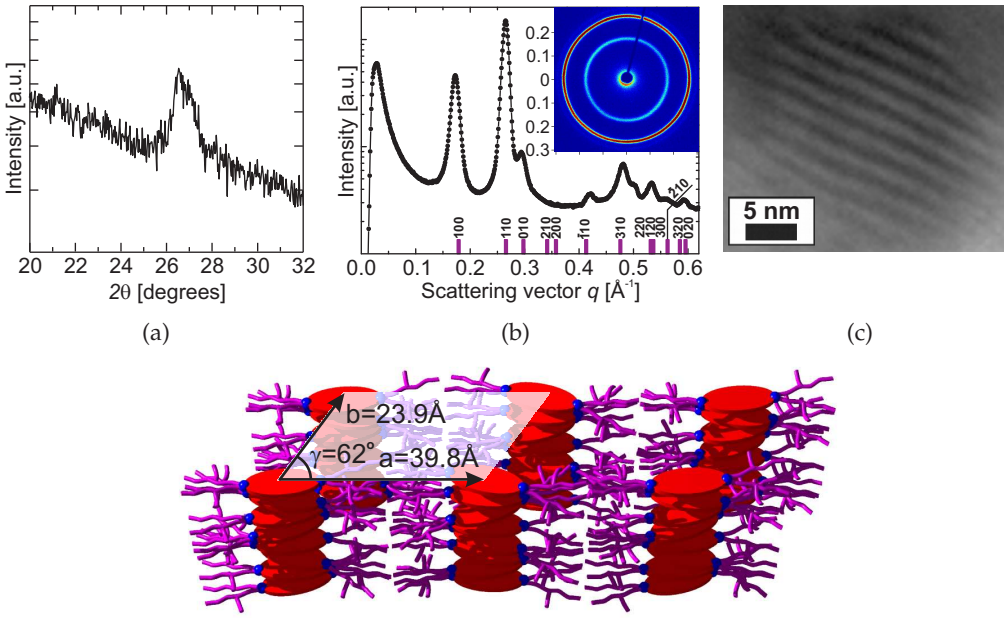

Figure 3.10. (a) WAXS and (b) SAXS intensity patterns from Pery-BEHP, where the positions of the reflections for the fitted structure are indicated ($a = 39.8$ Å, $b = 23.9$ Å, $\gamma = 62°$). (c) TEM micrograph from Pery-BEHP. (d) Scheme of the proposed oblique columnar structure. Reproduced with permission from **IV**. ©2008 Wiley-VCH Verlag GmbH & Co. KGaA.

material remained isotropic on the macroscopic length scale despite multiple attempts to achieve common macroscopic alignment by using oscillatory and steady shear flow. This characteristic is evidenced by the isotropic two-dimensional SAXS pattern in the inset of Figure 3.10(b). The degree of alignment can also be quantified by using the approach of Hermans[206] where an orientation factor f_z is calculated according to

$$f_z = 1 - \frac{3\int_0^{\pi/2} I(\phi)\sin^3\phi d\phi}{2\int_0^{\pi/2} I(\phi)\sin\phi d\phi}, \tag{3.10}$$

where $I(\phi)$ is the intensity along the azimuthal angle ϕ. The orientation factor $f_z = 1$ for a perfectly oriented structure and $f_z = 0$ for an isotropic Debye-ring arising from a randomly oriented structure. The orientation factor obtained from Figure 3.10(b) is $f_z \approx 0.06$ which means that the columns of Pery-BEHP are nearly randomly oriented and the material is macroscopically disordered and isotropic. One potential reason for the difficulty in obtaining mutual alignment in ISA materials might be the presence of the large number of charges in the ionic complexes that strongly suppress the structural reorganizations (required during the alignment process) due to the strong long-range Coulomb interactions. Therefore our hypothesis was that "dilution" of the charges in the ionic complexes through addition of nonpolar material could promote structural reorganizations during shear and could open practical routes toward overall alignment of the ISA materials. To test the hypothesis, the Pery-BEHP complexes were blended with different molecular weight polystyrenes (Table 3.1). Based on polarized optical microscopy and SAXS on the Pery-BEHP/PS blends, the Pery-BEHP was concluded to disperse in the PS matrix so that at least some of the dimensions of the Pery-BEHP aggregates are at the mesoscale. To align the Pery-BEHP columns, pellets of Pery-BEHP/PS blends were subjected to steady shear flow. Prior to shearing, the SAXS intensity patterns (Fig. 3.11) resembled those of the pure Pery-BEHP (Fig. 3.10(b)) i.e. possessed no macrocopic alignment. However, upon shearing, the alignment of the Pery-BEHP/PS blends systematically improves as a function of the molecular weight of the PS (Fig. 3.11). This improvement can once again be quantified using the approach of Hermans (Eq. 3.10) and the values of the orientation factor f_z for Pery-BEHP/PS blends constituting of different molecular weight PS are listed in Table 3.1.

The anisotropy of optically active materials is often expressed as a ratio in absorbance of polarized light at two different angles. To determine the values of

Table 3.1. Details of the polystyrenes used and values of the orientation factor f_z for shear aligned Pery-BEHP/PS samples as determined from the intensity patterns shown in Figure 3.11.

Sample	M_n(PS) [g mol^{-1}]	$M_w(PS)/M_n(PS)$	f_z
Pery-BEHP/PS1	6000	1.06	0.04
Pery-BEHP/PS2	24000	1.03	0.17
Pery-BEHP/PS3	50000	1.04	0.48
Pery-BEHP/PS4	115000	1.04	0.51

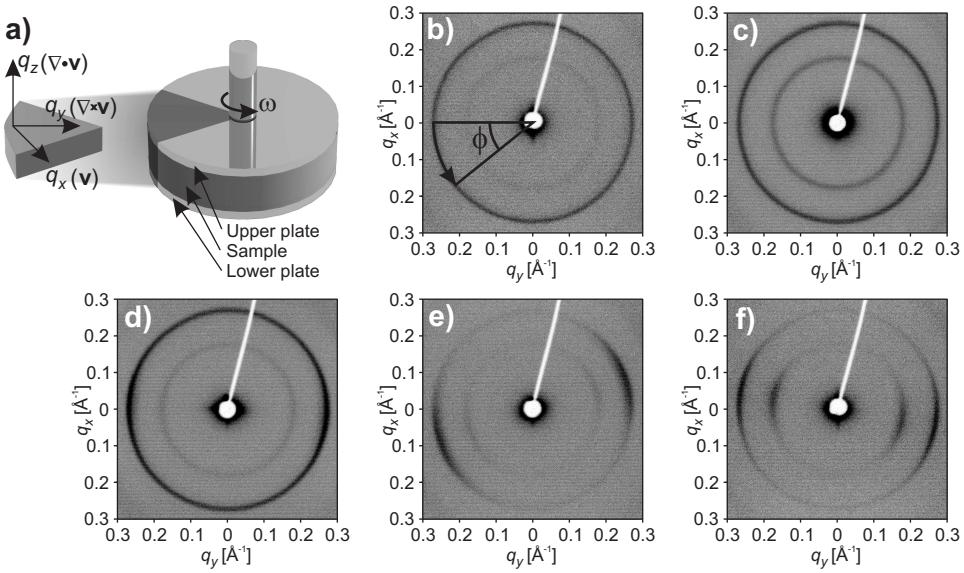

Figure 3.11. a) Scheme of the plate/plate geometry where the lower plate is fixed and the upper plate is rotated to produce shear flow to the sample between the parallel plates. The sample slice shows the corresponding coordinate axes where q_x is the direction of the flow field (v) and q_z shows the direction of the incident X-ray beam. SAXS intensity patterns for b) Pery-BEHP/PS4 sample prior to shear alignment showing also the azimuthal angle ϕ and SAXS intensity patterns for shear aligned c) Pery-BEHP/PS1, d) Pery-BEHP/PS2, e) Pery-BEHP/PS3 and f) Pery-BEHP/PS4. Reprinted with permission from **IV**. ©2008 Wiley-VCH Verlag GmbH & Co. KGaA.

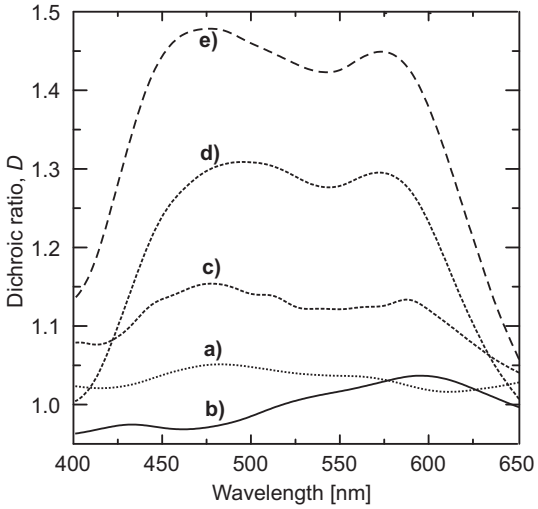

Figure 3.12. Dichroic ratio for a) Pery-BEHP/PS4 sample prior to shear alignment and for shear aligned b) Pery-BEHP/PS1, c) Pery-BEHP/PS2, d) Pery-BEHP/PS3, and e) Pery-BEHP/PS4, where the molecular weight of PS increases from 6000 g mol^{-1} (PS1) to 115000 g mol^{-1} (PS4). Reprinted with permission from **IV**. ©2008 Wiley-VCH Verlag GmbH & Co. KGaA.

this dichroic ratio for the aligned sample pellets, the absorbance of the plane polarized light was measured perpendicular ($A_\perp$) and parallel ($A_\parallel$) with respect to the flow direction (directions q_y and q_x, respectively, in Fig. 3.11). The dichroic ratios ($D(\lambda) = A_\perp(\lambda)/A_\parallel(\lambda)$) increase systematically as a function of the molecular weight of the blended PS in full agreement with the SAXS analysis (Fig. 3.12).

The alignment scheme is summarized in Figure 3.13. Blending Pery-BEHP with PS leads to high aspect ratio aggregates with mesoscale lateral dimensions, showing internal columnar LC order. Selecting PS with sufficiently high molecular weight, shearing leads to efficient alignment of the elongated LC aggregates at the mesoscale. As the LC aggregates, in turn, have well-defined internal self-assembled order, the shearing leads to high alignment of the perylenes at the molecular level, with macroscopic optical properties. Therefore, rather than trying to order the perylene molecules directly, we sooner shear align extended liquid-crystalline aggregates within a polymer matrix which better couples with the flow field.

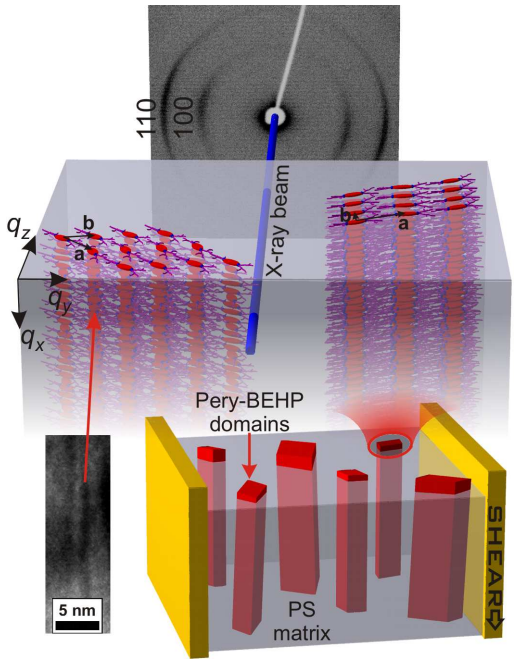

Figure 3.13. At the mesoscale the entangled matrix polymer chains align the elongated columnar liquid crystalline Pery-BEHP aggregates due to the flow field. The columnar liquid-crystalline aggregates, in turn, have well-defined internal columnar order, which leads to alignment of the optically active perylenes at the molecular level. Reprinted with permission from **IV**.

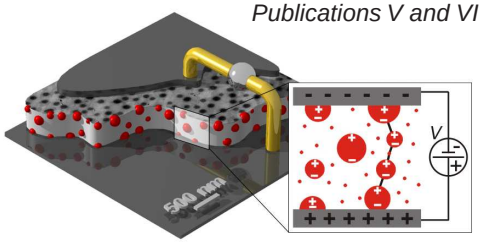

4 Nanocomposite memory elements

4.1 Background

One of the key objectives of today's information society is to provide quick and easy access to information - anywhere, anytime. Ubiquitous information requires development of unparalleled information storage technologies which possess such advantages as low cost and simplicity in fabrication and high mechanical flexibility of the devices but do not suffer from the limitations of conventional semiconductor electronics. A promising and rapidly emerging field that could answer to this challenge is organic electronics.[207–209] The potential of the field arises from the possibility to define the functionality at the molecular level and deposit the organic compound and therefore the electronics on a variety of surfaces from plastics to textiles and metal foils to form devices that are completely flexible.[208, 209] Although significant progress has been made in organic light-emitting diodes,[210–212] thin film transistors,[213–216] and photovoltaic cells,[217–219] the research on organic memory elements is still in its infancy.[220] A great number and variety of organic electronic devices have been reported to exhibit electrical switching and therefore proposed as the basis of organic memory elements.[221–234] Switching behavior alone, however, is insufficient and the devices must fulfill a full set of other demands associated with e.g. on-off ratio, write/read/erase time and cycling endurance in order to be fully exploited as memory elements.[220] In a recent critical review article, Scott and Bozano classified the materials and the proposed mechanisms that have been used in organic switching devices and they arrived at a conclusion that none of the reported devices satisfy the full set of demands.[220] To fully explore and exploit the potential of organic memory elements, the research must focus on clarifying the microscopic mechanism of switching and transport mechanism, optimizing the processes and materials and on excluding the effects that limit the reliability.[220, 235]

In Publications **V** and **VI** we strive to develop understanding of the working principles of organic nanocomposite memory elements and explore ways to tune the functionality of the devices by controlling the device morphology.

4.2 Electrical behavior

The design of the memory cells is a two-electrode sandwich structure in which the active nanocomposite layer of PS and a fullerene-derivative [6,6]-phenyl-C_{61} butyric acid methyl ester (PCBM, see Fig. 4.1(a)) is located between two parallel metal electrodes and deposited by solution coating. Figure 4.1(b) shows the typ-

ical electrical behavior of a PCBM/PS thin film device. In the first voltage scan (solid line in Fig. 4.1(b)), the current density increases by two orders of magnitude from the initial low current OFF state to high current ON state at V_{th} which is followed by negative differential resistance (NDR). In the subsequent voltage sweeps (dashed line in Fig. 4.1(b)) the device remains at the high current state. Absence of PCBM in the devices lead to completely different behavior with several orders of magnitude smaller current densities and absence of V_{th} and NDR as shown in Figure 4.1(b).

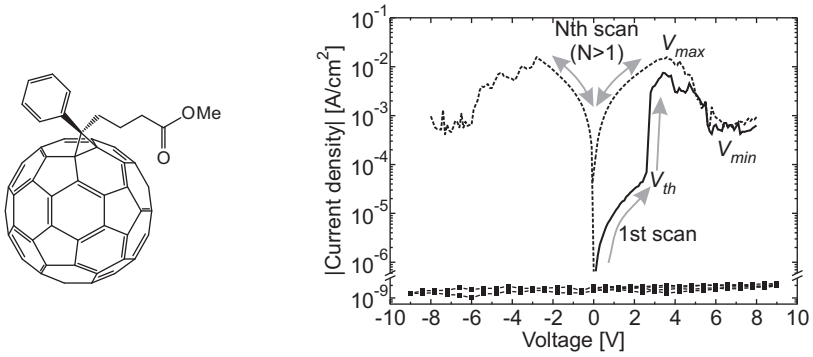

(a) (b)

Figure 4.1. (a) Fullerene-derivative [6,6]-phenyl-C_{61} butyric acid methyl ester i.e. PCBM. (b) Absolute value of the current density as a function of voltage for 5 wt% PCBM/PS (solid line for the first scan and dashed line for the subsequent scans) and 0 wt% PCBM/PS i.e. pure PS device (squares: ■). The active layer thicknesses are 250 nm and 210 nm for 5 wt% and 0 wt% PCBM/PS devices, respectively.

These results are against the recent argumentation which states that the electrodes in two terminal organic memory elements are the source for reversible switching whereas the organic material in between serves merely as a passive current limiting series resistance.[225, 236] In such studies, the switching and transport mechanism were explained based on presence of an oxide layer at the electrode and transport through *filaments*. This kind of *filamentary* conduction[237, 238] can take place when a metallic bridge connects the electrodes but local alignment of the storage medium can also lead to formation of high-mobility pathways which will give rise to the filamentary conduction. Furthermore, Tang *et al.* proposed that switching and NDR can be due to presence of metal nanoislands that form during the evaporation of the top electrode in the crevices of dust particles or other impurities present on the bottom electrode.

To clarify whether Al can penetrate into the active PCBM/PS layer during the evaporation of the electrodes and explain the observed electrical behavior, detailed knowledge of the device morphology is required.

4.3 Device morphology

Extensive TEM analysis were carried out on both unused and used Al-PCBM/PS-Al devices to answer whether Al can penetrate into the active PCBM/PS layer and to obtain a deeper understanding of the microscopic mechanism of switch-

ing and NDR. Figure 4.2 shows a plan view and cross-sectional TEM micrograph of a used 5 wt% PCBM/PS device. The micrographs do not show penetration of Al into the active medium and in addition the PCBM molecules seem to be homogenously dispersed in the polymer matrix as they do not show aggregation. Additionally, we performed energy dispersive X-ray spectroscopy (EDX) on the device cross-sections to determine conclusively the existence of Al in the active layer of the devices (Fig. 4.2). These results together with X-ray photoelectron spectroscopy[239] verify that the slow evaporation rate of Al (1.0-1.2 Å/s), used to fabricate the electrodes, does not lead to penetration of Al into the active PCBM/PS layer. In conclusion, the observation of the consistent NDR in the Al-PCBM/PS-Al devices (Fig. 4.1(b)) is less likely to be due to deliberate or unintentional inclusion of metal nanoparticles from the thermal evaporation of the Al electrodes and furthermore, introduction of the PCBM molecules into the PS matrix is a prerequisite for switching and NDR.

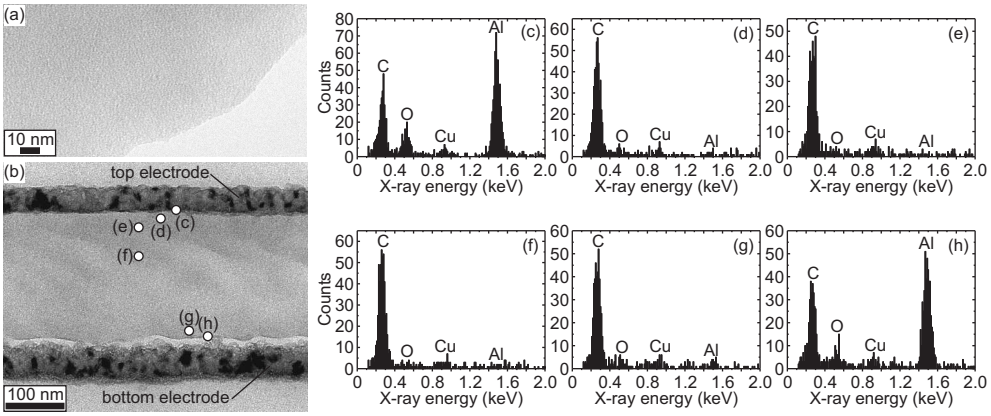

Figure 4.2. (a) Plan view TEM image of a used 5 wt% PCBM/PS device close to an edge (the thin film is on the left hand side of the image). (b) Cross-sectional TEM image of the same device consisting of a 250 nm thick 5 wt% PCBM/PS film sandwiched between the top and bottom Al electrodes. The spots used for the quantitative energy dispersive X-ray spectroscopy (EDX) analysis are indicated as circles in the cross-section and the corresponding results from the EDX analysis are shown in (c)-(h). Reprinted with permission from **V**. ©2008 Institute of Physics Publishing.

The above example shows that in order to understand the electrical behavior in thin film devices, it is relevant to study not only the plan view but also the cross-sectional morphology as the interfaces can have an effect on the morphology and therefore on the device characteristics. Most often, a combination of different experimental techniques is required to clarify conclusively the three-dimensional (3D) morphology of the thin films (Fig. 4.3). Knowledge of the 3D morphology will then form the basis for the models that can explain the corresponding device working mechanism. Atomic force microscopy (AFM) and scanning electron microscopy (SEM) offer excellent spatial resolution but they are sensitive only to surface features and incapable of detecting subsurface features, excluding some limiting cases.[240] TEM also lacks depth sensitivity as the two-dimensional transmission micrographs are averaged through the thickness of the 3D specimen even if 3D transmission electron tomography is applicable in some cases.[241]

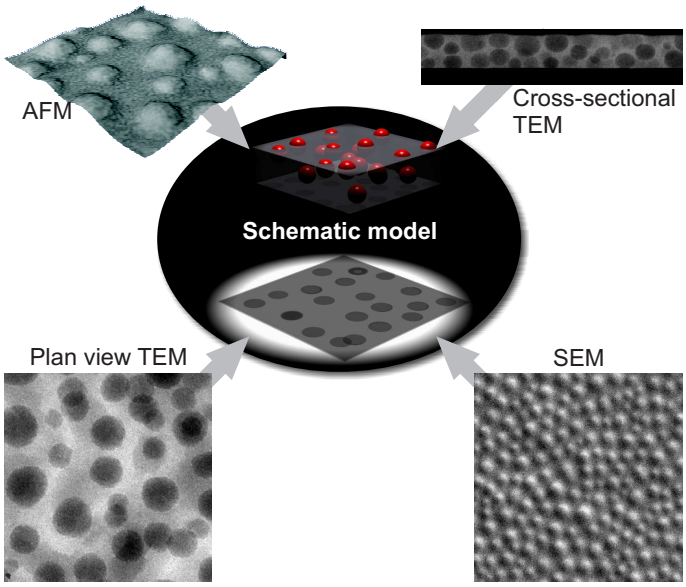

Figure 4.3. Nanocomposite structure and state of aggregation in annealed (120 °C) 40 wt% PCBM/PS thin films as evidenced by atomic force microscopy (AFM), scanning electron microscopy (SEM) and transmission electron microscopy (TEM). AFM image courtesy of Antti Soininen (TKK).

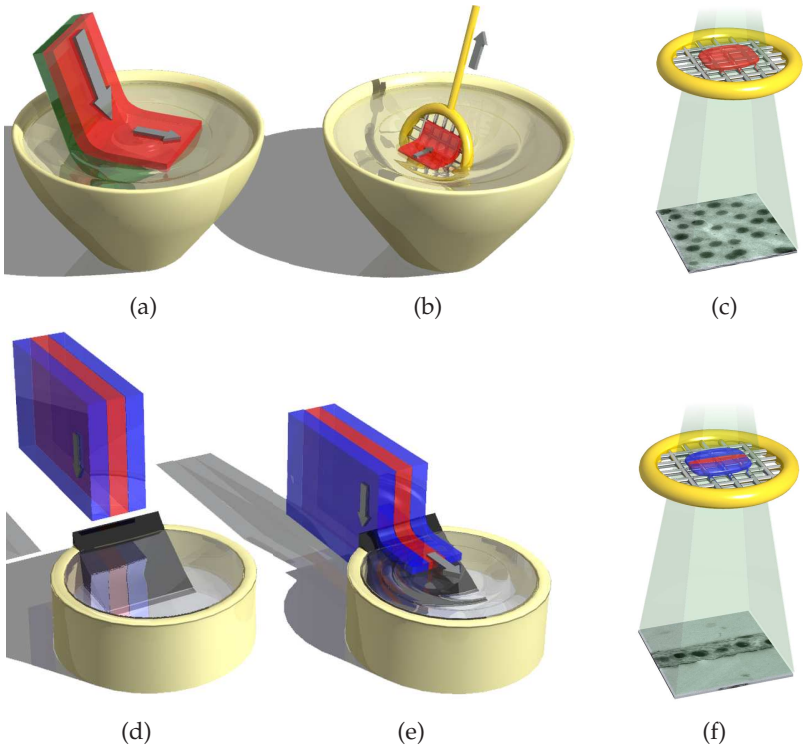

Figure 4.4. Sample preparation for plan view and cross-sectional TEM. For plan view TEM (a) the thin film (red) is first floated onto water surface and as a result the NaCl substrate (green) dissolves. (b) the thin film is then collected onto a TEM grid and (c) finally imaged with TEM. For cross-sectional TEM (d) the thin film (red) is first embedded and sandwiched between two epoxy layers (blue) and thereafter (e) ultra-microtomed to obtain thin sections transparent for (f) TEM imaging.

Combination of plan view and cross-sectional TEM, however, can provide the full 3D information required to build a complete model of the 3D structure (Publications **V** and **VI**). The sample preparation for plan view and cross-sectional TEM is summarized in Figure 4.4. For plan view TEM, the thin films are first spin coated onto NaCl substrates and subsequently floated off from the substrate onto water surface (Fig. 4.4(a)). Next the thin films are collected onto TEM grids (Fig. 4.4(b)) and finally imaged by TEM (Fig. 4.4(c)). We developed a corresponding sample preparation technique for cross-sectional TEM in which the thin film is embedded in epoxy and sectioned with an ultra-microtome (Fig. 4.4(d)-(e)) to yield TEM transparent thin sections (Fig. 4.4(f)).

4.4 Tuning the electrical behavior by control of morphology

In Publication **V** we studied the morphology of PCBM/PS thin films at low PCBM concentrations (<10 wt%) and reported well controlled morphology without visible aggregation at the resolution of TEM. In Publication **VI** we take this approach a step further and show that the device morphology can be controlled by the PCBM concentration and annealing which allows tuning of the electrical switching in PCBM/PS thin film devices.

In equilibrium, PCBM is expected to be prone to macroscopically phase separate from PS in PCBM/PS blends due to its high aggregation tendency. However, during a rapid spin coating process, the extent of phase separation within the glassy matrix can be limited by kinetic effects. Compositions that contain 10 wt% or less of PCBM with respect to PS are observed to lead to surprisingly homogenous films without a trace of aggregation (Fig. 4.5(a),(b)) within the resolution of the present TEM investigations where the smallest detectable particle size is ca. 20 nm. However, when the PCBM concentration exceeds ca. 20 wt%, TEM starts to indicate nanoscale phase separation of PCBM via nucleation and growth of spherical clusters as shown in Figure 4.5(c). Interestingly, the clusters systematically grow in size upon increasing the PCBM concentration.

The phase separation and formation of PCBM clusters depends strongly on the selected solvent for spin coating. Use of a low boiling point solvent like chloroform leads to nanoscale clusters (Fig. 4.5(c),(d)) whereas use of higher boiling point solvents such as toluene, chlorobenzene, and xylene led to phase separation at micrometer scale. Obviously the fast evaporation of low boiling point solvent during spin coating hinders large scale reorganization of the polymer chains before the glassy structure is frozen and thus phase separation occurs only at nanoscale. Note that the phase separation of PCBM in polymer matrices has already been widely investigated in the context of conjugated polymer/fullerene bulk heterojunction solar cells (for a recent review see[242]). We emphasize, however, that therein the matrix polymers are conjugated polymers, typically undergoing crystalline packing and PCBM clusters are much larger, and therefore such studies are of limited use in the present case with amorphous glassy polystyrene with nanoscale PCBM clusters.

In order to explore methods to control the PCBM aggregation, as well as the robustness of the process vs. the PCBM aggregation, the influence of thermal

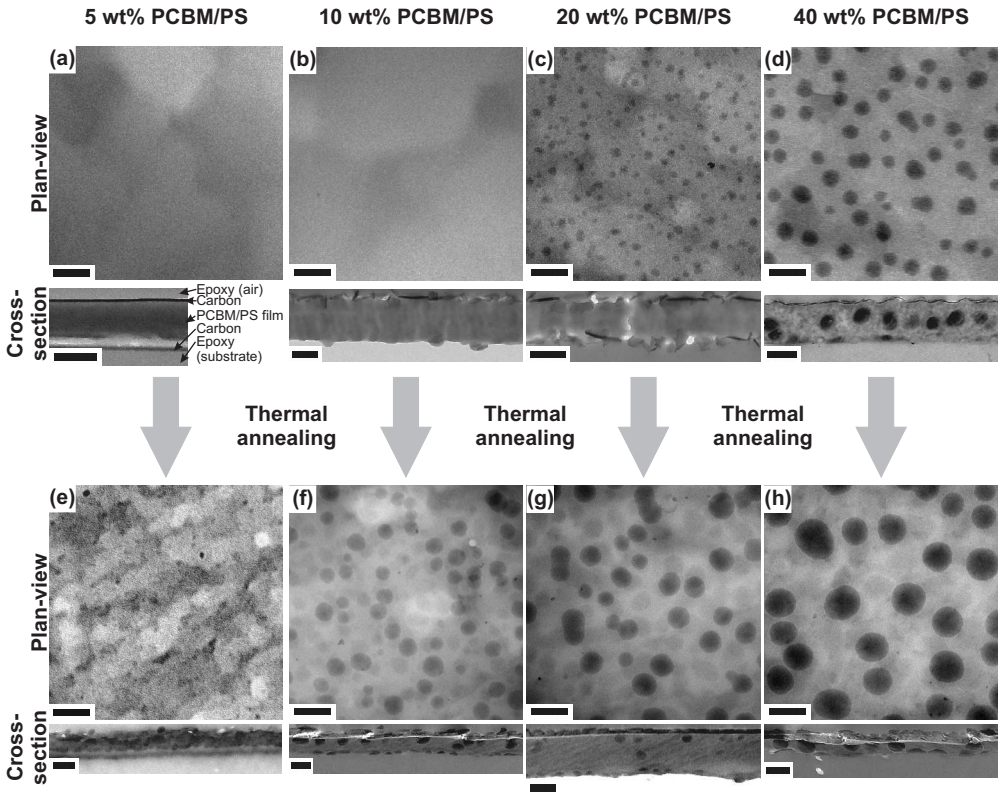

Figure 4.5. TEM micrographs showing the plan view (top) and cross-sectional view (bottom) for (a) 5 wt% (b) 10 wt% (c) 20 wt% (d) 40 wt% PCBM/PS thin films annealed at 80 °C for 90 minutes i.e. below T_g of PS and (e) 5 wt% (f) 10 wt% (g) 20 wt% (h) 40 wt% PCBM/PS thin films annealed at 120 °C for 90 minutes i.e. above T_g of PS. The top interface in the cross-sections is the air/film and the bottom film/substrate interface and to differentiate them better a thin layer of carbon has been evaporated onto both sides of the thin films. All scale bars are 200 nm. Reproduced with permission from **VI**. ©2008 American Institute of Physics.

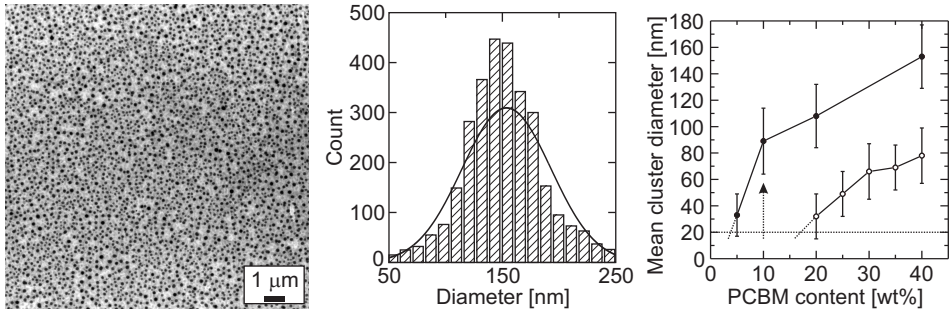

Figure 4.6. (a) TEM micrograph from 120°C annealed 40 wt% PCBM/PS and (b) the corresponding size distribution. (c) Mean cluster diameters in PCBM/PS thin films before (open symbols) and after thermal annealing at 120°C (closed symbols) as determined from the TEM micrographs. The error bars indicate the standard deviation. The smallest detectable particle size was ca. 20 nm. Reproduced with permission from **VI**. ©2008 American Institute of Physics.

treatment to the PCBM aggregation was studied by annealing the spin coated PCBM/PS thin films above the glass transition temperature of PS ($T_{g,PS} \approx 100$ °C). Annealing at 120 °C leads to increase in the cluster size as shown in Figures 4.5(e)-(h). The growth of the clusters is most clearly observable in the 10 wt% composition: prior to annealing (Fig. 4.5(b)) aggregation is not observed at the resolution of TEM, whereas annealing above $T_{g,PS}$ leads to appearance of clusters of roughly 90 nm in diameter (Fig. 4.5(f)).

Figure 4.6(c) shows mean cluster diameters together with the associated standard deviations for each PCBM/PS composition that have been determined from the plan view TEM micrographs using image processing and data analysis software. One can conclude from the figure that the average size of the clusters can be systematically controlled by merely changing the PCBM concentration and/or via thermal treatment. An important corollary is that if the high temperature annealing promotes growth of large PCBM clusters due to increased mobility of PCBM above the glass transition of PS, the fraction of finely dispersed PCBM, as not resolved in TEM, must decrease. Therefore the mutual distance of finely dispersed PCBM is expected to grow, which is expected to cause reduced electrical tunneling.

Having understood how to control the state of aggregation of PCBM in PS matrix, i.e. that fine dispersion of PCBM is promoted by low PCBM concentration, low boiling point solvent in spin coating, and low temperature processes, we next discuss the impact of the aggregation control on the electrical characteristics in devices where the active layer of PCBM/PS thin film has been sandwiched between two parallel aluminum electrodes. In the absence of PCBM, the pure PS devices exhibit only small leakage current without switching or NDR as shown in Figure 4.7(a). By contrast, adding only a small portion of PCBM (2 wt%) leads

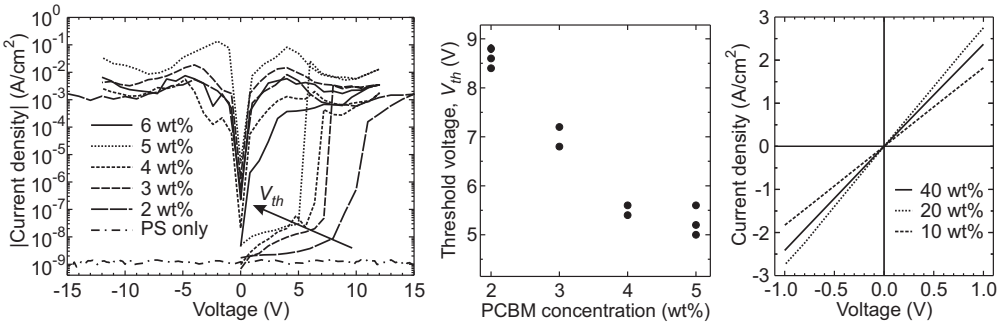

Figure 4.7. (a) Absolute current density as a function of voltage for pure polystyrene (PS, layer thickness $d = 200$ nm) and 2-6 wt% PCBM/PS compositions ($d = 250 - 260$ nm). (b) V_{th} as a function of PCBM concentration. (c) Current density as a function of voltage for 10-40 wt% PCBM/PS compositions ($d = 250$ nm), showing ohmic behavior. All devices have been annealed at 120 °C. Reprinted with permission from **VI**. ©2008 American Institute of Physics.

to switching of the current by 6-7 orders of magnitude from the initial low current off state to high current on state at ca. 9 V (Fig. 4.7(a)). This switching is followed by NDR in the subsequent voltage sweeps. Increasing PCBM concentrations up to 5 wt% allow to tune the switching voltage from ca. 9 to 5 V (Fig.

4.7(b)). Above ca. 7 wt% Ohmic I-V curves are observed instead of switching or NDR, starting from the first voltage sweep at voltages as low as 1 mV, indicating that the device is short circuited (Fig. 4.7(c)). The electrical behavior above ca. 7 wt% PCBM concentration receives a natural explanation if we take a look at the underlying morphology (Fig. 4.5(f)-(h)). The PCBM clusters can now form electrically connected chains of clusters from one electrode to the other and thus short circuit the aluminum electrodes. Moreover, the current levels scale linearly with the area of the overlap between the electrodes as shown in Figure 4.8(a). This is further evidence against the local filamentary conduction[243] as being the reason for the electrical behavior in such PCBM/PS devices.

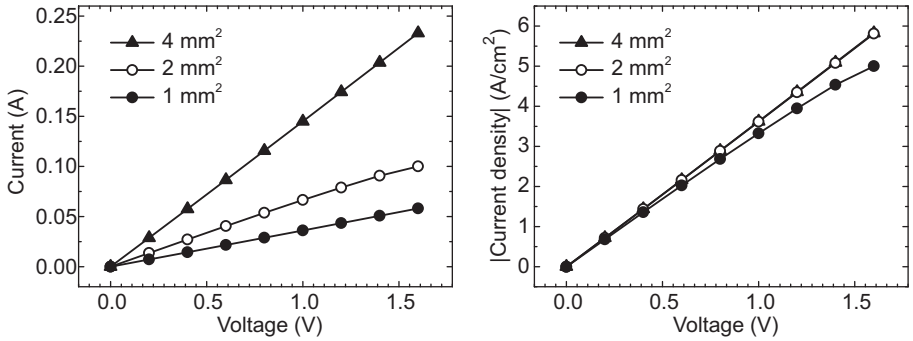

Figure 4.8. (a) Current vs. voltage curves for 10 wt% PCBM/PS composition with different device areas. (b) Absolute current densities as a function of voltage for the same devices.

We will next propose a model to explain the switching behavior below 6 wt% PCBM/PS concentration. Let us model the aggregated PCBM/PS system with two homogenous dielectric spheres ($\epsilon_{PCBM} = 3.9$, Ref. [244]) that are placed into another dielectric medium ($\epsilon_{PS} = 2.6$). The problem is to solve the strength of the electric field in the vicinity of the two spheres when an initially uniform and constant electric field ($\boldsymbol{E_0}$) parallel to the axis of the two spheres is introduced. This problem is most easily expressed in a bispherical coordinate system[245]

$$x = \frac{a \sin\alpha \cos\phi}{\cosh\eta - \cos\alpha} \tag{4.1}$$

$$y = \frac{a \sin\alpha \sin\phi}{\cosh\eta - \cos\alpha} \tag{4.2}$$

$$z = \frac{a \sinh\eta}{\cosh\eta - \cos\alpha}, \tag{4.3}$$

where the parameter a is the length of a tangent from the origin to one of the spheres, $a = \sqrt{l^2 - R^2}$, R is the radius of the spheres and $z_0 = \pm l$ is the position of the centers of the spheres. The solution to this electrostatic problem is given by solving the corresponding Laplace's equation in the bispherical coordinate

system

$$\nabla^2 V = \frac{(\cosh\eta - \cos\alpha)^3}{a^2 \sin\alpha}\left[\sin\alpha\frac{\partial}{\partial\eta}\left(\frac{1}{\cosh\eta - \cos\alpha}\frac{\partial V}{\partial\eta}\right) + \frac{\partial}{\partial\alpha}\left(\frac{\sin\alpha}{\cosh\eta - \cos\alpha}\frac{\partial V}{\partial\alpha}\right) + \frac{1}{\sin\alpha(\cosh\eta - \cos\alpha)}\frac{\partial^2 V}{\partial^2\phi}\right] = 0. \quad (4.4)$$

The general solution to equation 4.4 is given by

$$V = \sqrt{\cosh\eta - \cos\alpha}\sum_{n=0}^{\infty}(M_n e^{(n+\frac{1}{2})\eta} + N_n e^{-(n+\frac{1}{2})\eta})P_n(\cos\alpha), \quad (4.5)$$

where $P_n(\cos\alpha)$ is Legendre function of the first kind. Incorporation of the boundary conditions[†] to equation 4.5 leads to a set of difference equations which can be solved by using the approach of Goyette and Navon.[246] The corresponding electric field ($\boldsymbol{E}$) is then given by the negative gradient of the potential, $\boldsymbol{E} = -\nabla V$ and finally, the graphical representation of the solution is shown in Figure 4.9(a). The polarization of the PCBM clusters obviously leads to increase in the strength

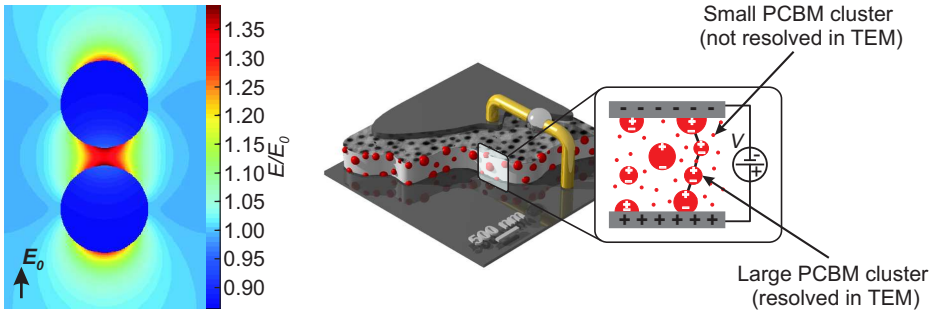

(a) (b)

Figure 4.9. (a) Strength of the electric field in the vicinity of two dielectric spheres where an initially uniform electric field (E_0) is applied. (b) Combination of a TEM micrograph and a schematic illustration showing the polarization between the PCBM clusters, separated by the PS matrix. Reproduced with permission from **VI**. ©2008 American Institute of Physics.

of the electric field between adjacent clusters which can explain the observed device behavior. Though the origin of V_{th} might be explained by the model that assumes the presence of a thin insulating oxide layer at the semiconductor/metal interface,[236] that model is unable to explain the presently observed shift of V_{th} (Fig. 4.7(b)) and absence of switching for 0 wt% (Fig. 4.7(a)) and $>$ 7 wt% (Fig. 4.7(c)). However, the polarization of the PCBM clusters and generation of a stronger electric field between adjacent clusters along the direction of the electric field could account for these effects as schematically shown in Fig. 4.9(b).

Furthermore, in Publication **VI** we suggest that the NDR is an outcome of the tunneling process between the PCBM clusters. The NDR is similar to what has been observed in *electroformed* devices by Simmons and Verderber[247] and later

[†]Continuity of the potential and dielectric displacement across the interface of the spheres, and $\lim_{z\to\infty} V = V_0$, where $V_0 = -E_0 z$ is the potential due to the external field.

by Thurstans and Oxley[248] where inclusion of metal into the dielectric or semiconductor material under the influence of electric field has been clarified as the reason for this phenomenon. Since we have shown the absence of metal inclusion in the PCBM/PS devices, the PCBM clusters in the PS matrix must act as the *formed* islands and give rise to the NDR with the added advantage that the PCBM aggregation can be controlled by the PCBM concentration and annealing, unlike the field-induced formed metal. Finally, we have shown strong evidence that breakdown of the native aluminum oxide layer cannot solely explain the observed device behavior. The results on different device morphologies and their relation to the electrical behavior suggest, on the contrary, that PCBM/PS layer does not merely act as a passive current limiting series resistance but it also has a strong influence on the device behavior and allows tuning of switching and NDR.

5 Conclusions

In this thesis, we have presented novel pathways, on one hand, to control the formation of nanoscale polymeric structures to obtain further functions and, on the other hand, to align the locally ordered structures over macroscopic dimensions.

In Publication **I** we demonstrated how supramolecular chemistry and block copolymer self-assembly can be used in a facile way to direct the assembly of C_{60} fullerenes. Incorporation of the C_{60} molecules into block copolymer systems led to unexpected self-assembled morphologies in both bulk and spin coated thin films, when the copolymer contained electron donating moieties that can form charge-transfer complexes with the electron-accepting C_{60} molecules. We further proposed that charge-transfer complexation may become essential to understand some of the self-assembled structures of C_{60}, and they can, when used in a rational way, lead to novel pathways for the construction of self-assembled fullerene containing materials and tuning of the functions.

Publications **II**-**IV** dealt with the alignment of randomly oriented domains of nanoscale structures over macroscopic length scales - a common issue often encountered in self-assembled but only locally ordered soft matter. Construction of a real-time rheo-optical apparatus and the use of rheo-optics to elucidate the alignment dynamics of block copolymer systems was demonstrated. Alignment of randomly oriented domains is not only useful for obtaining macroscopically anisotropic materials and functions, but it can also be a prerequisite for detailed characterization of the local structures. This was further indicated in Publication **III** where we reported coexistence of parallel and perpendicular orientation of smectic layers within copolymer lamellae in a side chain liquid crystalline block copolymer. Parallel orientation of the smectic layers has earlier been thought to exist in bulk only if long alkyl spacers connect the mesogens to the polymer backbone, whereas we showed that parallel alignment can be achieved in a shear aligned system bearing only a short ethyl spacer. Moreover, the fraction of the parallel orientation could be controlled by oscillation frequency and shear strain amplitude. Use of supramolecular chemistry and ionic self-assembly (ISA) was shown to allow facile combination of various functionalities in a modular fashion by complexing charged functional moieties with ionic surfactants. In spite of the promise of ISA as a source of modular materials for, e.g., optical and electrical applications, their overall alignment has remained a challenge, in particular when aiming at a technically feasible and straightforward process. In Publication **IV**, we introduced a facile scheme that can allow overall alignment of the ISA complexes beyond the local polydomain-like order. The scheme was based on blending the ISA complexes with a high molecular weight inert polymer and

then aligning the ISA complexes within the polymer matrix by subjecting the blend to shear flow at elevated temperatures. Selecting a polymer with sufficiently high molecular weight, shearing was shown to lead to efficient alignment of the elongated liquid crystalline aggregates at the mesoscale. As the aggregates, in turn, have well-defined internal self-assembled order, the shearing leads to high alignment of the ISA complexes on the molecular scale, with macroscopic optical properties.

In Publications **V** and **VI**, control of nanoscale morphology was shown to allow tuning of the electrical switching in polymer/fullerene nanocomposite thin film devices that could be used as organic memory elements. The working principles of such thin film organic memory devices have remained debated and tunability has been less presented. Also encouraged by a more general need to promote materials scientific understanding of nanocomposite thin film devices, the first systematic approach was undertaken to tailor the active material composition and to study the morphology by TEM specifically in the cross-sectional direction in relation to the devices. The electrical behavior of the devices was found to fall into three different categories: *i) switching from a high resistance state to a low resistance state at V_{th} in the first voltage sweep.* The position of V_{th} could be tuned by varying the PCBM concentration. V_{th} was suggested to result from the polarization of the PCBM clusters and generation of a stronger electric field between adjacent clusters. *ii) Negative differential resistance (NDR) in subsequent repeated voltage cycles.* Unintentional inclusion of Al into the active nanocomposite layer during the evaporation of the electrodes and its possibility of explaining the observed NDR could be excluded based on the electrical measurements on pristine polymer devices and quantitative elemental analysis from the device cross-sections. The NDR was associated to similar effects observed in "electroformed" devices with the added advantage that the PCBM clusters play the role of "formed" metal electrodes and can be controlled by the PCBM concentration and annealing, unlike the field-induced "formed" metal. *iii) Ohmic behavior.* High PCBM concentration led to short-circuiting due to formation of cluster chains or single large clusters that could couple the electrodes. Finally, we showed strong evidence that breakdown of the native aluminum oxide layer at the electrodes cannot solely explain the observed device behavior. The results on different device morphologies and their relation to the electrical behavior suggest, on the contrary, that the nanocomposite layer does not merely act as a passive current limiting series resistance but it also has a strong influence on the device behavior and allows tuning of switching and NDR.

References

[1] Austin, M. D., Ge, H. X., Wu, W., Li, M. T., Yu, Z. N., Wasserman, D., Lyon, S. A. & Chou, S. Y. Fabrication of 5 nm linewidth and 14 nm pitch features by nanoimprint lithography. *Appl. Phys. Lett.* **84**, 5299 (2004).

[2] Lehn, J. M. Toward self-organization and complex matter. *Science* **295**, 2400 (2002).

[3] Hawker, C. J. & Russell, T. P. Block copolymer lithography: Merging "bottom-up" with "top-down" processes. *MRS Bull.* **30**, 952 (2005).

[4] Hamley, I. W. *The Physics of Block Copolymers* (Oxford University Press, Oxford, 1998).

[5] Förster, S. & Antonietti, M. Amphiphilic block copolymers in structure-controlled nanomaterial hybrids. *Adv. Mater.* **10**, 195 (1998).

[6] Bates, F. S. & Fredrickson, G. H. Block copolymers - designer soft materials. *Phys. Today* **52**, 32 (1999).

[7] Förster, S. & Plantenberg, T. From self-organizing polymers to nanohybrid and biomaterials. *Angew. Chem. Int. Ed.* **41**, 689 (2002).

[8] Hadjichristidis, N., Pispas, S. & Floudas, G. *Block Copolymers: Synthetic Strategies, Physical Properties, and Applications* (Wiley, New York, 2002).

[9] Hamley, I. W. Nanostructure fabrication using block copolymers. *Nanotechnology* **14**, R39 (2003).

[10] Matsen, M. W. The standard gaussian model for block copolymer melts. *J. Phys.: Condens. Matter* **14**, R21 (2002).

[11] Hamley, I. W. Structure and flow behaviour of block copolymers. *J. Phys.: Condens. Matter* **13**, R643 (2001).

[12] Lopes, W. A. & Jaeger, H. M. Hierarchical self-assembly of metal nanostructures on diblock copolymer scaffolds. *Nature* **414**, 735 (2001).

[13] Sohn, B. H. & Seo, B. H. Fabrication of the multilayered nanostructure of alternating polymers and gold nanoparticles with thin films of self-assembling diblock copolymers. *Chem. Mater.* **13**, 1752 (2001).

[14] Chai, J. & Buriak, J. M. Using cylindrical domains of block copolymers to self-assemble and align metallic nanowires. *ACS Nano* **2**, 489 (2008).

[15] Lee, J. Y., Shou, Z. & Balazs, A. C. Modeling the self-assembly of copolymer-nanoparticle mixtures confined between solid surfaces. *Phys. Rev. Lett.* **91** (2003).

[16] Lin, Y., Boker, A., He, J. B., Sill, K., Xiang, H. Q., Abetz, C., Li, X. F., Wang, J., Emrick, T., Long, S., Wang, Q., Balazs, A. & Russell, T. P. Self-directed self-assembly of nanoparticle/copolymer mixtures. *Nature* **434**, 55 (2005).

[17] He, J. B., Tangirala, R., Emrick, T., Russell, T. P., Boker, A., Li, X. F. & Wang, J. Self-assembly of nanoparticle-copolymer mixtures: A kinetic point of view. *Adv. Mater.* **19**, 381 (2007).

[18] Lee, J. Y., Thompson, R. B., Jasnow, D. & Balazs, A. C. Effect of nanoscopic particles on the mesophase structure of diblock copolymers. *Macromolecules* **35**, 4855 (2002).

[19] Sun, Y. S., Jeng, U. S., Liang, K. S., Yeh, S. W. & Wei, K. H. Transitions of domain ordering and domain size in a spherical-forming polystyrene-block-poly(ethylene oxide) copolymer and its composites with colloidal cadmium sulfide quantum dots. *Polymer* **47**, 1101 (2006).

[20] Kim, B. J., Chiu, J. J., Yi, G. R., Pine, D. J. & Kramer, E. J. Nanoparticle-induced phase transitions in diblock-copolymer films. *Adv. Mater.* **17**, 2618 (2005).

[21] Yeh, S. W., Wei, K. H., Sun, Y. S., Jeng, U. S. & Liang, K. S. CdS nanoparticles induce a morphological transformation of poly(styrene-b-4-vinylpyridine) from hexagonally packed cylinders to a lamellar structure. *Macromolecules* **38**, 6559 (2005).

[22] Warren, S. C., Disalvo, F. J. & Wiesner, U. Nanoparticle-tuned assembly and disassembly of mesostructured silica hybrids. *Nat. Mater.* **6**, 156 (2007).

[23] Kim, B. J., Fredrickson, G. H., Hawker, C. J. & Kramer, E. J. Nanoparticle surfactants as a route to bicontinuous block copolymer morphologies. *Langmuir* **23**, 7804 (2007).

[24] Warren, S. C., Messina, L. C., Slaughter, L. S., Kamperman, M., Zhou, Q., Gruner, S. M., DiSalvo, F. J. & Wiesner, U. Ordered mesoporous materials from metal nanoparticle-block copolymer self-assembly. *Science* **320**, 1748 (2008).

[25] Balazs, A. C., Emrick, T. & Russell, T. P. Nanoparticle polymer composites: Where two small worlds meet. *Science* **314**, 1107 (2006).

[26] Fujita, N., Yamashita, T., Asai, M. & Shinkai, S. Formation of [60]fullerene nanoclusters

with controlled size and morphology through the aid of supramolecular rodcoil diblock copolymers. *Angew. Chem. Int. Ed.* **44**, 1257 (2005).
[27] Kroto, H. W., Heath, J. R., O'Brien, S. C., Curl, R. F. & Smalley, R. E. C_{60}: Buckminsterfullerene. *Nature* **318**, 162 (1985).
[28] Kroto, H. W. *Symmetry, space, stars and C60* (Nobel Lecture, 1996).
[29] Osawa, E. K. Superaromaticity. *Kagaku (Kyoto)* **25**, 854 (1970).
[30] Bochvar, D. A. & Gal'pern, E. G. Hypothetical systems: Carbododecahedron, s-icosahedron, and carbo-s-icosahedron. *Dokl. Akad. Nauk SSSR* **209**, 610 (1973).
[31] Jones (Daedalus), D. E. H. Hollow molecules. *New Scientist* **32**, 245 (1966).
[32] Kratschmer, W., Lamb, L. D., Fostiropoulos, K. & Huffman, D. R. Solid C-60 - a new form of carbon. *Nature* **347**, 354 (1990).
[33] Wragg, J. L., Chamberlain, J. E., White, H. W., Kratschmer, W. & Huffman, D. R. Scanning tunneling microscopy of solid C-60/C-70. *Nature* **348**, 623 (1990).
[34] Kratschmer, W., Fostiropoulos, K. & Huffman, D. R. The infrared and ultraviolet-absorption spectra of laboratory-produced carbon dust - evidence for the presence of the C-60 molecule. *Chem. Phys. Lett.* **170**, 167 (1990).
[35] Ajie, H., Alvarez, M. M., Anz, S. J., Beck, R. D., Diederich, F., Fostiropoulos, K., Huffman, D. R., Kratschmer, W., Rubin, Y., Schriver, K. E., Sensharma, D. & Whetten, R. L. Characterization of the soluble all-carbon molecules C60 and C70. *J. Phys. Chem.* **94**, 8630 (1990).
[36] Haddon, R. C., Brus, L. E. & Raghavachari, K. Rehybridization and pi-orbital alignment - the key to the existence of spheroidal carbon clusters. *Chem. Phys. Lett.* **131**, 165 (1986).
[37] Haddon, R. C., Brus, L. E. & Raghavachari, K. Electronic-structure and bonding in icosahedral C-60. *Chem. Phys. Lett.* **125**, 459 (1986).
[38] Tutt, L. W. & Kost, A. Optical limiting performance of C-60 and C-70 solutions. *Nature* **356**, 225 (1992).
[39] Kajzar, F., Taliani, C., Danieli, R., Rossini, S. & Zamboni, R. Wave-dispersed 3rd-order nonlinear-optical properties of C-60 thin-films. *Chem. Phys. Lett.* **217**, 418 (1994).
[40] Haddon, R. C., Perel, A. S., Morris, R. C., Palstra, T. T. M., Hebard, A. F. & Fleming, R. M. C-60 thin-film transistors. *Appl. Phys. Lett.* **67**, 121 (1995).
[41] Haddon, R. C., Hebard, A. F., Rosseinsky, M. J., Murphy, D. W., Duclos, S. J., Lyons, K. B., Miller, B., Rosamilia, J. M., Fleming, R. M., Kortan, A. R., Glarum, S. H., Makhija, A. V., Muller, A. J., Eick, R. H., Zahurak, S. M., Tycko, R., Dabbagh, G. & Thiel, F. A. Conducting films of C60 and C70 by alkali-metal doping. *Nature* **350**, 320 (1991).
[42] Hebard, A. F., Rosseinsky, M. J., Haddon, R. C., Murphy, D. W., Glarum, S. H., Palstra, T. T. M., Ramirez, A. P. & Kortan, A. R. Superconductivity at 18-K in potassium-doped C-60. *Nature* **350**, 600 (1991).
[43] Grant, P. Superconductivity - up on the C-60 elevator. *Nature* **413**, 264 (2001).
[44] Allemand, P. M., Khemani, K. C., Koch, A., Wudl, F., Holczer, K., Donovan, S., Gruner, G. & Thompson, J. D. Organic molecular soft ferromagnetism in a fullerene-C60. *Science* **253**, 301 (1991).
[45] Lappas, A., Prassides, K., Vavekis, K., Arcon, D., Blinc, R., Cevc, P., Amato, A., Feyerherm, R., Gygax, F. N. & Schenck, A. Spontaneous magnetic-ordering in the fullerene charge-transfer salt (TDAE)C-60. *Science* **267**, 1799 (1995).
[46] Narymbetov, B., Omerzu, A., Kabanov, V. V., Tokumoto, M., Kobayashi, H. & Mihailovic, D. Origin of ferromagnetic exchange interactions in a fullerene-organic compound. *Nature* **407**, 883 (2000).
[47] Mizoguchi, K., Machino, M., Sakamoto, H., Kawamoto, T., Tokumoto, M., Omerzu, A. & Mihailovic, D. Pressure effect in TDAE-C-60 ferromagnet: Mechanism and polymerization. *Phys. Rev. B* **6314** (2001).
[48] Ruoff, R. S., Tse, D. S., Malhotra, R. & Lorents, D. C. Solubility of C-60 in a variety of solvents. *J. Phys. Chem.* **97**, 3379 (1993).
[49] Taylor, R. & Walton, D. R. M. The chemistry of fullerenes. *Nature* **363**, 685 (1993).
[50] Hirsch, A. The chemistry of the fullerenes - an overview. *Angew. Chem. Int. Ed.* **32**, 1138 (1993).
[51] Diederich, F. & Thilgen, C. Covalent fullerene chemistry. *Science* **271**, 317 (1996).
[52] Prato, M. [60]fullerene chemistry for materials science applications. *J. Mater. Chem.* **7**, 1097 (1997).
[53] Geckeler, K. & Samal, S. Featured article syntheses and properties of macromolecular fullerenes, a review. *Polym. Int.* **48**, 743 (1999).

[54] Mignard, E., Hiorns, R. & Francois, B. Synthesis and characterization of star copolymers consisting of fullerene and conjugated polyphenylene: 6-star-C60[styrene-poly(1,4-phenylene)-block-polystyrene] and 6-star-C60[polystyrene-block-poly(1,4-phenylene)]. *Macromolecules* **35**, 6132 (2002).
[55] Wudl, F. Fullerene materials. *J. Mater. Chem.* **12**, 1959 (2002).
[56] Wang, C., Guo, Z.-X., Fu, S., Wu, W. & Zhu, D. Polymers containing fullerene or carbon nanotube structures. *Progress Polym. Sci.* **29**, 1079 (2004).
[57] Olah, G. A., Bucsi, I., Lambert, C., Aniszfeld, R., Trivedi, N. J., Sensharma, D. K. & Prakash, G. K. S. Considered polycarbon supercage chemistry .3. polyarenefullerenes, C60(H-AR)n, obtained by acid-catalyzed fullerenation of aromatics. *J. Am. Chem. Soc.* **113**, 9387 (1991).
[58] Loy, D. A. & Assink, R. A. Synthesis of a C-60-p-xylylene copolymer. *J. Am. Chem. Soc.* **114**, 3977 (1992).
[59] Kojima, Y., Matsuoka, T., Takahashi, H. & Kurauchi, T. Optical limiting property of polystyrene-bound C-60. *Macromolecules* **28**, 8868 (1995).
[60] Geckeler, K. E. & Hirsch, A. Polymer-bound C-60. *J. Am. Chem. Soc.* **115**, 3850 (1993).
[61] Bergbreiter, D. E. & Gray, H. N. Grafting of C-60 onto polyethylene surfaces. *J. Chem. Soc.-Chem. Commun.* 645 (1993).
[62] Manolova, N., Rashkov, I., Beguin, F. & Vandamme, H. Amphiphilic derivatives of fullerenes formed by polymer modification. *J. Chem. Soc.-Chem. Commun.* 1725 (1993).
[63] Shi, S., Khemani, K. C., Li, Q. C. & Wudl, F. A polyester and polyurethane of diphenyl-C61 - retention of fulleroid properties in a polymer. *J. Am. Chem. Soc.* **114**, 10656 (1992).
[64] Zhang, N. J., Schricker, S. R., Wudl, F., Prato, M., Maggini, M. & Scorrano, G. A new C-60 polymer via ring-opening metathesis polymerization. *Chem. Mater.* **7**, 441 (1995).
[65] Wooley, K. L., Hawker, C. J., Frechet, J. M. J., Wudl, F., Srdanov, G., Shi, S., Li, C. & Kao, M. Fullerene-bound dendrimers - soluble, isolated carbon clusters. *J. Am. Chem. Soc.* **115**, 9836 (1993).
[66] Hawker, C. J., Wooley, K. L. & Frechet, J. M. J. Dendritic fullerenes - a new approach to polymer modification of C-60. *J. Chem. Soc.-Chem. Commun.* 925 (1994).
[67] Jenekhe, S. A. & Chen, X. L. Self-assembled aggregates of rod-coil block copolymers and their solubilization and encapsulation of fullerenes. *Science* **279**, 1903 (1998).
[68] Chen, X. L. & Jenekhe, S. A. Solubilization and encapsulation of fullerenes by amphiphilic block copolymers. *Langmuir* **15**, 8007 (1999).
[69] Schmaltz, B., Brinkmann, M. & Mathis, C. Nanoscale organization of fullerenes by self-assembly in a diblock copolymer host matrix. *Macromolecules* **37**, 9056 (2004).
[70] Yu, H., Gan, L. H., Hu, X., Venkatraman, S. S., Tam, K. C. & Gang, Y. Y. A novel amphiphilic double-[60]fullerene-capped triblock copolymer. *Macromolecules* **38**, 9889 (2005).
[71] Sivula, K., Ball, Z. T., Watanabe, N. & Frechet, J. M. J. Amphiphilic diblock copolymer compatibilizers and their effect on the morphology and performance of polythiophene: Fullerene solar cells. *Adv. Mater.* **18**, 206 (2006).
[72] Barrau, S., Heiser, T., Richard, F., Brochon, C., Ngov, C., van de Wetering, K., Hadziioannou, G., Anokhin, D. V. & Ivanov, D. A. Self-assembling of novel fullerene-grafted donor-acceptor rod-coil block copolymers. *Macromolecules* **41**, 2701 (2008).
[73] Stalmach, U., de Boer, B., Videlot, C., van Hutten, P. F. & Hadziioannou, G. Semiconducting diblock copolymers synthesized by means of controlled radical polymerization techniques. *J. Am. Chem. Soc.* **122**, 5464 (2000).
[74] Nierengarten, J.-F., Guttierez-Nava, M., Zhang, S., Masson, P., Oswald, L., Bourgogne, C., Rio, Y., Accorsi, G., Armaroli, N. & Setayesh, S. Fullerene-containing macromolecules for materials science applications. *Carbon* **42**, 1077 (2004).
[75] Ball, Z. T., Sivula, K. & Frechet, J. M. J. Well-defined fullerene-containing homopolymers and diblock copolymers with high fullerene content and their use for solution-phase and bulk organization. *Macromolecules* **39**, 70 (2006).
[76] Huang, X.-D., Goh, S., Lee, S. & Huan, C. Complexation between hydrogensulfated fullerenol and poly(4-vinylpyridine). *Macromol. Chem. Phys.* **201**, 281 (2000).
[77] Cheng, J.-x., Fang, Y., Huang, Q.-j., Yan, Y.-J. & Li, X.-Y. Blue-green photoluminescence from pyridine-C60 adduct. *Chem. Phys. Lett.* **330**, 262 (2000).
[78] Bhattacharya, S., Nayak, S., Chattopadhyay, S., Banerjee, M. & Mukherjee, A. Study of molecular complex formation between [60]fullerene and two series of donors by the NMR method. *J. Phys. Chem. A* **105**, 9865 (2001).
[79] Bhattacharya, S., Banerjee, M. & Mukherjee, A. Absorption spectrometric study of molecular

complex formation between [60]fullerene and a series of methylated pyridines. *Spectrochim Acta, A* **58A**, 2563 (2002).

[80] Mizuseki, H., Igarashi, N., Belosludov, R. V., Farajian, A. A. & Kawazoe, Y. Theoretical study of phthalocyanine-fullerene complex for a high efficiency photovoltaic device using ab initio electronic structure calculation. *Synth. Met.* **138**, 281 (2003).

[81] Bhattacharya, S., Bhattacharya, S. C. & Banerjee, M. Spectrophotometric studies of complexation of Safranine T and Safranine O with [60]- and [70]fullerenes and other electron acceptors. *J. Phys. Chem. A* **108**, 10783 (2004).

[82] Bhattacharya, S. & Banerjee, M. Spectrophotometric and thermodynamic studies of complexation of [60]fullerene with a series of anisoles: a rational approach towards charge transfer interaction. *Chem. Phys. Lett.* **396**, 377 (2004).

[83] Zhao, Y. & Fang, Y. Fluorescence of C60 and its interaction with pyridine. *J. Phys. Chem. B* **108**, 13586 (2004).

[84] Arias, F., Echegoyen, L., Wilson, S. R., Lu, Q. & Lu, Q. Y. Methanofullerenes and methanofulleroids have different electrochemical-behavior at negative potentials. *J. Am. Chem. Soc.* **117**, 1422 (1995).

[85] Echegoyen, L. & Echegoyen, L. E. Electrochemistry of fullerenes and their derivatives. *Acc. Chem. Res.* **31**, 593 (1998).

[86] Yeh, S. W., Chang, Y. T., Chou, C. H. & Wei, K. H. Effect of surface-hydroxylated CdS nanoparticles on the morphological transformation of polystyrene-block-poly(ethylene oxide) thin films. *Macromol. Rapid Commun.* **25**, 1680 (2004).

[87] Zhang, H. F., Hussain, I., Brust, M., Butler, M. F., Rannard, S. P. & Cooper, A. I. Aligned two- and three-dimensional structures by directional freezing of polymers and nanoparticles. *Nat. Mater.* **4**, 787 (2005).

[88] Olson, D. A., Chen, L. & Hillmyer, M. A. Templating nanoporous polymers with ordered block copolymers. *Chem. Mater.* **20**, 869 (2008).

[89] Singh, D. K., Krotkov, R. V., Xiang, H. Q., Xu, T., Russell, T. P. & Tuominen, M. T. Arrays of ultrasmall metal rings. *Nanotechnology* **19** (2008).

[90] Segalman, R. A., Yokoyama, H. & Kramer, E. J. Graphoepitaxy of spherical domain block copolymer films. *Adv. Mater.* **13**, 1152 (2001).

[91] Harrison, C., Cheng, Z. D., Sethuraman, S., Huse, D. A., Chaikin, P. M., Vega, D. A., Sebastian, J. M., Register, R. A. & Adamson, D. H. Dynamics of pattern coarsening in a two-dimensional smectic system. *Phys. Rev. E* **66**, 011706 (2002).

[92] Segalman, R. A., Hexemer, A., Hayward, R. C. & Kramer, E. J. Ordering and melting of block copolymer spherical domains in 2 and 3 dimensions. *Macromolecules* **36**, 3272 (2003).

[93] Segalman, R. A., Schaefer, K. E., Fredrickson, G. H., Kramer, E. J. & Magonov, S. Topographic templating of islands and holes in highly asymmetric block copolymer films. *Macromolecules* **36**, 4498 (2003).

[94] Harrison, C., Angelescu, D. E., Trawick, M., Cheng, Z. D., Huse, D. A., Chaikin, P. M., Vega, D. A., Sebastian, J. M., Register, R. A. & Adamson, D. H. Pattern coarsening in a 2D hexagonal system. *Europhys. Lett.* **67**, 800 (2004).

[95] Vega, D. A., Harrison, C. K., Angelescu, D. E., Trawick, M. L., Huse, D. A., Chaikin, P. M. & Register, R. A. Ordering mechanisms in two-dimensional sphere-forming block copolymers. *Phys. Rev. E* **71**, 061803 (2005).

[96] Cheng, J. Y., Ross, C. A., Smith, H. I. & Thomas, E. L. Templated self-assembly of block copolymers: Top-down helps bottom-up. *Adv. Mater.* **18**, 2505 (2006).

[97] Mansky, P., DeRouchey, J., Russell, T. P., Mays, J., Pitsikalis, M., Morkved, T. & Jaeger, H. Large-area domain alignment in block copolymer thin films using electric fields. *Macromolecules* **31**, 4399 (1998).

[98] Schaffer, E., Thurn-Albrecht, T., Russell, T. P. & Steiner, U. Electrically induced structure formation and pattern transfer. *Nature* **403**, 874 (2000).

[99] Boker, A., Knoll, A., Elbs, H., Abetz, V., Muller, A. H. E. & Krausch, G. Large scale domain alignment of a block copolymer from solution using electric fields. *Macromolecules* **35**, 1319 (2002).

[100] Boker, A., Elbs, H., Hansel, H., Knoll, A., Ludwigs, S., Zettl, H., Urban, V., Abetz, V., Muller, A. H. E. & Krausch, G. Microscopic mechanisms of electric-field-induced alignment of block copolymer microdomains. *Phys. Rev. Lett.* **89**, 135502 (2002).

[101] Ferri, D., Wolff, D., Springer, J., Francescangeli, O., Laus, M., Sante Angeloni, A., Galli, G. & Chiellini, E. Phase and orientational behaviors in liquid crystalline main-chain/side-group

block copolymers. *J. Polym. Sci., Part B: Polym. Phys.* **36**, 21 (1998).
[102] Hamley, I. W., Castelletto, V., Lu, Z. B., Imrie, C. T., Itoh, T. & Al-Hussein, M. Interplay between smectic ordering and microphase separation in a series of side-group liquid-crystal block copolymers. *Macromolecules* **37**, 4798 (2004).
[103] Osuji, C., Ferreira, P. J., Mao, G., Ober, C. K., Vander Sande, J. B. & Thomas, E. L. Alignment of self-assembled hierarchical microstructure in liquid crystalline diblock copolymers using high magnetic fields. *Macromolecules* **37**, 9903 (2004).
[104] Grigorova, T., Pispas, S., Hadjichristidis, N. & Thurn-Albrecht, T. Magnetic field induced orientation in diblock copolymers with one crystallizable block. *Macromolecules* **38**, 7430 (2005).
[105] Keller, A., Pedemonte, E. & Willmouth, F. M. Macro-lattice from segregated amorphous phases of a three block copolymer. *Nature* **225**, 538 (1970).
[106] Folkes, M. J., Keller, A. & Scalisi, F. P. Extrusion technique for the preparation of single crystals of block copolymers. *Colloid. Polym. Sci.* **257**, 136 (1973).
[107] Hadziioannou, G., Mathis, A. & Skoulios, A. Preparation of "single crystals" of three-block styrene/isoprene/styrene copolymers by plane shearing. *Colloid. Polym. Sci.* **257**, 136 (1979).
[108] Morrison, F. A. & Winter, H. H. The effect of unidirectional shear on the structure of triblock copolymers. I. polystyrene-polybutadiene-polystyrene. *Macromolecules* **22**, 3533 (1989).
[109] Morrison, F. A., Mays, J. W., Muthukumar, M., Nakatani, A. I. & Han, C. C. Shear-induced morphological structures in triblock copolymers. *Macromolecules* **26**, 5271 (1993).
[110] Koppi, K. A., Tirrell, M., Bates, F. S., Almdal, K. & Colby, R. H. Lamellae orientation in dynamically sheared diblock copolymer melts. *J. Phys. II* **2**, 1941 (1992).
[111] Koppi, K. A., Tirrell, M. & Bates, F. S. Shear-induced isotropic-to-lamellar transition. *Phys. Rev. Lett.* **70**, 1449 (1993).
[112] Koppi, K. A., Tirrell, M., Bates, F. S., Almdal, K. & Mortensen, K. Epitaxial growth and shearing of the body centered cubic phase in diblock copolymer melts. *J. Rheol.* **38**, 999 (1994).
[113] Tepe, T., Hajduk, D. A., Hillmyer, M. A., Weimann, P. A., Tirrell, M., Bates, F. S., Almdal, K. & Mortensen, K. Influence of shear on a lamellar triblock copolymer near the order-disorder transition. *J. Rheol.* **41**, 1147 (1997).
[114] Vigild, M. E., Chu, C., Sugiyama, M., Chaffin, K. A. & Bates, F. S. Influence of shear on the alignment of a lamellae-forming pentablock copolymer. *Macromolecules* **34**, 951 (2001).
[115] Chen, Z. R., Kornfield, J. A., Smith, S. D., Grothaus, J. T. & Satkowski, M. M. Pathways to macroscale order in nanostructured block copolymers. *Science* **277**, 1248 (1997).
[116] Chen, Z. R. & Kornfield, J. A. Flow-induced alignment of lamellar block copolymer melts. *Polymer* **39**, 4679 (1998).
[117] Gupta, V. K., Krishnamoorti, R., Kornfield, J. A. & Smith, S. D. Evolution of microstructure during shear alignment in a polystyrene-polyisoprene lamellar diblock copolymer. *Macromolecules* **28**, 4464 (1995).
[118] Gupta, V. K., Krishnamoorti, R., Kornfield, J. A. & Smith, S. D. Role of strain in controlling lamellar orientation during flow alignment of diblock copolymers. *Macromolecules* **29**, 1359 (1996).
[119] Gupta, V. K., Krishnamoorti, R., Chen, Z. R., Kornfield, J. A., Smith, S. D., Satkowski, M. M. & Grothaus, J. T. Dynamics of shear alignment in a lamellar diblock copolymer: Interplay of frequency, strain amplitude, and temperature. *Macromolecules* **29**, 875 (1996).
[120] Leist, H., Maring, D., Thurn-Albrecht, T. & Wiesner, U. Double flip of orientation for a lamellar diblock copolymer under shear. *J. Chem. Phys.* **110**, 8225 (1999).
[121] Zhang, Y. M. & Wiesner, U. Symmetrical diblock copolymers under large-amplitude oscillatory shear-flow - entanglement effect. *J. Chem. Phys.* **103**, 4784 (1995).
[122] Zhang, Y. M., Wiesner, U., Yang, Y. L., Pakula, T. & Spiess, H. W. Annealing effects on orientation in dynamically sheared diblock copolymers. *Macromolecules* **29**, 5427 (1996).
[123] Zhang, Y. M. & Wiesner, U. Symmetric diblock copolymers under large amplitude oscillatory shear flow: Dual frequency experiments. *J. Chem. Phys.* **106**, 2961 (1997).
[124] Maring, D. & Wiesner, U. Threshold strain value for perpendicular orientation in dynamically sheared diblock copolymers. *Macromolecules* **30**, 660 (1997).
[125] Polis, D. L., Smith, S. D., Terrill, N. J., Ryan, A. J., Morse, D. C. & Winey, K. I. Shear-induced lamellar rotation observed in a diblock copolymer by in situ small-angle X-ray scattering. *Macromolecules* **32**, 4668 (1999).
[126] Pinheiro, B. S. & Winey, K. I. Mixed parallel-perpendicular morphologies in diblock copoly-

mer systems correlated to the linear viscoelastic properties of the parallel and perpendicular morphologies. *Macromolecules* **31**, 4447 (1998).
[127] Patel, S. S., Larson, R. G., Winey, K. I. & Watanabe, H. Shear orientation and rheology of a lamellar polystyrene polyisoprene block-copolymer. *Macromolecules* **28**, 4313 (1995).
[128] Winey, K. I., Patel, S. S., Larson, R. G. & Watanabe, H. Interdependence of shear deformations and block copolymer morphology. *Macromolecules* **26**, 2542 (1993).
[129] Wang, H., Kesani, P. K., Balsara, N. P. & Hammouda, B. Undulations and disorder in block copolymer lamellae under shear flow. *Macromolecules* **30**, 982 (1997).
[130] Wang, H., Newstein, M. C., Krishnan, A., Balsara, N. P., Garetz, B. A., Hammouda, B. & Krishnamoorti, R. Ordering kinetics and alignment of block copolymer lamellae under shear flow. *Macromolecules* **32**, 3695 (1999).
[131] Riise, B. L., Fredrickson, G. H., Larson, R. G. & Pearson, D. S. Rheology and shear-induced alignment of lamellar diblock and triblock copolymers. *Macromolecules* **28**, 7653 (1995).
[132] Hermel, T. J., Wu, L. F., Hahn, S. F., Lodge, T. P. & Bates, F. S. Shear-induced lamellae alignment in matched triblock and pentablock copolymers. *Macromolecules* **35**, 4685 (2002).
[133] Okamoto, S., Saijo, K. & Hashimoto, T. Real-time SAXS observations of lamella-forming block-copolymers under large oscillatory shear deformation. *Macromolecules* **27**, 5547 (1994).
[134] Okamoto, S., Saijo, K. & Hashimoto, T. Dynamic SAXS studies of sphere-forming block-copolymers under large oscillatory shear deformation. *Macromolecules* **27**, 3753 (1994).
[135] Pople, J. A., Hamley, I. W. & Diakun, G. P. An integrated couette system for in situ shearing of polymer and surfactant solutions and gels with simultaneous small angle X-ray scattering. *Rev. Sci. Instrum.* **69**, 3015 (1998).
[136] Vigild, M. E., Almdal, K., Mortensen, K., Hamley, I. W., Fairclough, J. P. A. & Ryan, A. J. Transformations to and from the gyroid phase in a diblock copolymer. *Macromolecules* **31**, 5702 (1998).
[137] Kannan, R. M. & Kornfield, J. A. Evolution of microstructure and viscoelasticity during flow-alignment of a lamellar diblock copolymer. *Macromolecules* **27**, 1177 (1994).
[138] Chen, Z. R., Issaian, A. M., Kornfield, J. A., Smith, S. D., Grothaus, J. T. & Satkowski, M. M. Dynamics of shear-induced alignment of a lamellar diblock: A rheo-optical, electron microscopy, and X-ray scattering study. *Macromolecules* **30**, 7096 (1997).
[139] Wilhelm, M., Maring, D. & Spiess, H. W. Fourier-transform rheology. *Rheol. Acta* **37**, 399 (1998).
[140] Langela, M., Wiesner, U., Spiess, H. W. & Wilhelm, M. Microphase reorientation in block copolymer melts as detected via FT rheology and 2D SAXS. *Macromolecules* **35**, 3198 (2002).
[141] Kliger, D. S., Lewis, J. W. & Randall, C. E. *Polarized Light in Optics and Spectroscopy* (Academic Press, Inc., San Diego, 1990).
[142] Brosseau, C. *Fundamentals of polarized light: a statistical optics approach* (John Wiley & Sons, Inc., New York, 1998).
[143] Allan, P., Arridge, R. G. C., Ehtaiatkar, F. & Folkes, M. J. The mechanical-properties of an oriented lamella stock formed from an S-B-S block copolymer. *J. Phys. D: Appl. Phys.* **24**, 1381 (1991).
[144] Lodge, T. P. & Fredrickson, G. H. Optical anisotropy of tethered chains. *Macromolecules* **25**, 5643 (1992).
[145] de Gennes, P. G. & Prost, J. *The Physics of Liquid Crystals* (Oxford University Press, New York, 1998), 2nd edn.
[146] Kumar, S. *Liquid Crystals* (Cambridge University Press, Cambridge, 2001).
[147] Kato, T. Self-assembly of phase-segregated liquid crystal structures. *Science* **295**, 2414 (2002).
[148] Kato, T., Mizoshita, N. & Kishimoto, K. Functional liquid-crystalline assemblies: Self-organized soft materials. *Angew. Chem. Int. Ed.* **45**, 38 (2006).
[149] Plate, N. A. & Shibaev, V. P. *Comb-Shaped Polymers and Liquid Crystals* (Plenum Press, New York, 1987).
[150] McCardle, C. B. *Side Chain Liquid Crystalline Polymers* (Chapman and Hall, New York, 1989).
[151] Shibaev, V. P. & Lam, L. *Liquid Crystalline and Mesomorphic Polymers* (Springer-Verlag, New York, 1994).
[152] Rendon, S., Burghardt, W. R., Auad, M. L. & Kornfield, J. A. Shear-induced alignment of smectic side group liquid crystalline polymers. *Macromolecules* **40**, 6624 (2007).
[153] Shah, M., Pryarnitsyn, V. & Ganesan, V. A model for self-assembly in side chain liquid crystalline block copolymers. *Macromolecules* **41**, 218 (2008).
[154] Verploegen, E., Zhang, T., Murlo, N. & Hammond, P. T. Influence of variations in liquid-

crystalline content upon the self-assembly behavior of siloxane-based block copolymers. *Soft Matter* **4**, 1279 (2008).

[155] Mao, G. P., Wang, J. G., Clingman, S. R., Ober, C. K., Chen, J. T. & Thomas, E. L. Molecular design, synthesis, and characterization of liquid crystal coil diblock copolymers with azobenzene side groups. *Macromolecules* **30**, 2556 (1997).

[156] Yamada, M., Iguchi, T., Hirao, A., Nakahama, S. & Watanabe, J. Synthesis of side-chain liquid-crystalline homopolymers and block copolymers with well-defined structures by living anionic-polymerization and their thermotropic phase-behavior. *Macromolecules* **28**, 50 (1995).

[157] Al-Hussein, M., de Jeu, W. H., Vranichar, L., Pispas, S., Hadjichristidis, N., Itoh, T. & Watanabe, J. Bulk and thin film ordering in side-chain liquid-crystalline/amorphous diblock copolymers: The role of chain length. *Macromolecules* **37**, 6401 (2004).

[158] Hamley, I. W., Castelletto, V., Parras, P., Lu, Z. B., Imrie, C. T. & Itoh, T. Ordering on multiple lengthscales in a series of side group liquid crystal block copolymers containing a cholesteryl-based mesogen. *Soft Matter* **1**, 355 (2005).

[159] Zheng, W. Y., Albalak, R. J. & Hammond, P. T. Mesogen orientation within smectic C* side chain liquid crystalline diblock copolymers. *Macromolecules* **31**, 2686 (1998).

[160] Anthamatten, M., Zheng, W. Y. & Hammond, P. T. A morphological study of well-defined smectic side-chain LC block copolymers. *Macromolecules* **32**, 4838 (1999).

[161] Anthamatten, M. & Hammond, P. T. Free-energy model of asymmetry in side-chain liquid-crystalline diblock copolymers. *J. Polym. Sci., Part B: Polym. Phys.* **39**, 2671 (2001).

[162] Ruokolainen, J., Makinen, R., Torkkeli, M., Makela, T., Serimaa, R., ten Brinke, G. & Ikkala, O. Switching supramolecular polymeric materials with multiple length scales. *Science* **280**, 557 (1998).

[163] Ruokolainen, J., ten Brinke, G. & Ikkala, O. Supramolecular polymeric materials with hierarchical structure-within-structure morphologies. *Adv. Mater.* **11**, 777 (1999).

[164] Schneider, A., Zanna, J. J., Yamada, M., Finkelmann, H. & Thomann, R. Competition between liquid crystalline phase symmetry and microphase morphology in a chiral smectic liquid crystalline-isotropic block copolymer. *Macromolecules* **33**, 649 (2000).

[165] Thunemann, A. F. & General, S. Poly(ethylene oxide)-b-polyethylene imine) dodecanoate complexes: Lamellar-within-lamellar morphologies and nanoparticles. *Macromolecules* **34**, 6978 (2001).

[166] Tsao, C. S. & Chen, H. L. Concurrent transformation of copolymer domain morphology induced by the order-disorder transition of comb block in supramolecular comb-coil block copolymer. *Macromolecules* **37**, 8984 (2004).

[167] Nandan, B., Lee, C. H., Chen, H. L. & Chen, W. C. Molecular architecture effect on the microphase separations in supramolecular comb-coil complexes of polystyrene-block-poly(2-vinylpyridine) with dodecylbenzenesulfonic acid: (AB)(n)A(n) block-arm star copolymer. *Macromolecules* **38**, 10117 (2005).

[168] Valkama, S., Ruotsalainen, T., Kosonen, H., Ruokolainen, J., Torkkeli, M., Serimaa, R., ten Brinke, G. & Ikkala, O. Amphiphiles coordinated to block copolymers as a template for mesoporous materials. *Macromolecules* **36**, 3986 (2003).

[169] Osuji, C., Chao, C. Y., Bita, I., Ober, C. K. & Thomas, E. L. Temperature-dependent photonic bandgap in a self-assembled hydrogen-bonded liquid-crystalline diblock copolymer. *Adv. Funct. Mater.* **12**, 753 (2002).

[170] Valkama, S., Ruotsalainen, T., Nykanen, A., Laiho, A., Kosonen, H., ten Brinke, G., Ikkala, O. & Ruokolainen, J. Self-assembled structures in diblock copolymers with hydrogen-bonded amphiphilic plasticizing compounds. *Macromolecules* **39**, 9327 (2006).

[171] Kosonen, H., Valkama, S., Ruokolainen, J., Torkkeli, M., Serimaa, R., ten Brinke, G. & Ikkala, O. One-dimensional optical reflectors based on self-organization of polymeric comb-shaped supramolecules. *European Physical Journal E* **10**, 69 (2003).

[172] Ikkala, O. & ten Brinke, G. Hierarchical self-assembly in polymeric complexes: Towards functional materials. *Chem. Commun.* 2131 (2004).

[173] Valkama, S., Kosonen, H., Ruokolainen, J., Haatainen, T., Torkkeli, M., Serimaa, R., Ten Brinke, G. & Ikkala, O. Self-assembled polymeric solid films with temperature-induced large and reversible photonic-bandgap switching. *Nat. Mater.* **3**, 872 (2004).

[174] Faul, C. F. J. & Antonietti, M. Ionic self-assembly: Facile synthesis of supramolecular materials. *Adv. Mater.* **15**, 673 (2003).

[175] Wurthner, F. Perylene bisimide dyes as versatile building blocks for functional supramolec-

ular architectures. *Chem. Commun.* 1564 (2004).
[176] Guan, Y., Zakrevskyy, Y., Stumpe, J., Antonietti, M. & Faul, C. F. J. Perylenediimide-surfactant complexes: thermotropic liquid-crystalline materials via ionic self-assembly. *Chem. Commun.* 894 (2003).
[177] Zakrevskyy, Y., Faul, C. F. J., Guan, Y. & Stumpe, J. Alignment of a perylene-based ionic self-assembly complex in thermotropic and lyotropic liquid-crystalline phases. *Adv. Funct. Mater.* **14**, 835 (2004).
[178] Schmidt-Mende, L., Fechtenkotter, A., Mullen, K., Moons, E., Friend, R. H. & MacKenzie, J. D. Self-organized discotic liquid crystals for high-efficiency organic photovoltaics. *Science* **293**, 1119 (2001).
[179] Wurthner, F., Chen, Z. J., Hoeben, F. J. M., Osswald, P., You, C. C., Jonkheijm, P., von Herrikhuyzen, J., Schenning, A. P. H. J., van der Schoot, P. P. A. M., Meijer, E. W., Beckers, E. H. A., Meskers, S. C. J. & Janssen, R. A. J. Supramolecular p-n-heterojunctions by co-self-organization of oligo(p-phenylene vinylene) and perylene bisimide dyes. *J. Am. Chem. Soc.* **126**, 10611 (2004).
[180] Wurthner, F., Thalacker, C., Diele, S. & Tschierske, C. Fluorescent J-type aggregates and thermotropic columnar mesophases of perylene bisimide dyes. *Chem.-Eur. J.* **7**, 2245 (2001).
[181] Makinen, R., Ruokolainen, J., Ikkala, O., de Moel, K., ten Brinke, G., De Odorico, W. & Stamm, M. Orientation of supramolecular self-organized polymeric nanostructures by oscillatory shear flow. *Macromolecules* **33**, 3441 (2000).
[182] de Moel, K., Maki-Ontto, R., Stamm, M., Ikkala, O. & ten Brinke, G. Oscillatory shear flow-induced alignment of lamellar melts of hydrogen-bonded comb copolymer supramolecules. *Macromolecules* **34**, 2892 (2001).
[183] Maki-Ontto, R., de Moel, K., Polushkin, E., van Ekenstein, G. A., ten Brinke, G. & Ikkala, O. Tridirectional protonic conductivity in soft materials. *Adv. Mater.* **14**, 357 (2002).
[184] Polushkin, E., van Ekenstein, G. A., Dolbnya, I., Bras, W., Ikkala, O. & ten Brinke, G. In situ radial small angle synchrotron X-ray scattering study of shear-induced macroscopic orientation of hierarchically structured comb-shaped supramolecules. *Macromolecules* **36**, 1421 (2003).
[185] Ruotsalainen, T., Torkkeli, M., Serimaa, R., Makela, T., Maki-Ontto, R., Ruokolainen, J., ten Brinke, G. & Ikkala, O. Structural hierarchy in flow-aligned hexagonally self-organized microphases with parallel polyelectrolytic structures. *Macromolecules* **36**, 9437 (2003).
[186] van Ekenstein, G. A., Polushkin, E., Nijland, H., Ikkala, O. & ten Brinke, G. Shear alignment at two length scales: Comb-shaped supramolecules self-organized as cylinders-within-lamellar hierarchy. *Macromolecules* **36**, 3684 (2003).
[187] Polushkin, E., van Ekenstein, G. A., Ikkala, O. & ten Brinke, G. A modified rheometer for in-situ radial and tangential SAXS studies on shear-induced alignment. *Rheol. Acta* **43**, 364 (2004).
[188] Polushkin, E., Bondzic, S., de Wit, J., van Ekenstein, G. A., Dolbnya, I., Bras, W., Ikkala, O. & ten Brinke, G. In-situ SAXS study on the alignment of ordered systems of comb-shaped supramolecules: A shear-induced cylinder-to-cylinder transition. *Macromolecules* **38**, 1804 (2005).
[189] Bondzic, S., Polushkin, E., Schouten, A. J., Ikkala, O. & ten Brinke, G. The influence of grain size on the alignment of hexagonally ordered cylinders of self-assembled diblock copolymer-based supramolecules. *Polymer* **48**, 4723 (2007).
[190] Faul, C., Antonietti, M., Sanderson, R. & Hentze, H. P. Directed polymerization in mesophases of polyelectrolyte-surfactant complexes. *Langmuir* **17**, 2031 (2001).
[191] Faul, C. F. J. & Antionietti, M. Facile synthesis of optically functional, highly organized nanostructures: Dye-surfactant complexes. *Chem.-Eur. J.* **8**, 2764 (2002).
[192] Guan, Y., Antonietti, M. & Faul, C. F. J. Ionic self-assembly of dye-surfactant complexes: Influence of tail lengths and dye architecture on the phase morphology. *Langmuir* **18**, 5939 (2002).
[193] Camerel, F., Antonietti, M. & Faul, C. F. J. Organized nanostructured complexes of inorganic clusters and surfactants that exhibit thermal solid-state transformations. *Chem.-Eur. J.* **9**, 2160 (2003).
[194] Camerel, F. & Faul, C. F. J. Combination of ionic self-assembly and hydrogen bonding as a tool for the synthesis of liquid-crystalline materials and organogelators from a simple building block. *Chem. Commun.* 1958 (2003).
[195] Ganeva, D., Antonietti, M., Faul, C. F. J. & Sanderson, R. Polymerization of the organized

phases of polyelectrolyte-surfactant complexes. *Langmuir* **19**, 6561 (2003).
[196] Faul, C. F. J. Structure-function relationship in optically and electronically active ISA materials. *Synth. Met.* **147**, 63 (2004).
[197] Kadam, J., Faul, C. F. J. & Scherf, U. Induced liquid crystallinity in switchable side-chain discotic molecules. *Chem. Mater.* **16**, 3867 (2004).
[198] Guan, Y., Yu, S. H., Antonietti, M., Bottcher, C. & Faul, C. F. J. Synthesis of supramolecular polymers by ionic self-assembly of oppositely charged dyes. *Chem.-Eur. J.* **11**, 1305 (2005).
[199] Zhang, T. R., Spitz, C., Antonietti, M. & Faul, C. F. J. Highly photoluminescent polyoxometaloeuropate-surfactant complexes by ionic self-assembly. *Chem.-Eur. J.* **11**, 1001 (2005).
[200] Faul, C. F. J. Liquid-crystalline materials by the ionic self-assembly route. *Mol. Cryst. Liquid Cryst.* **450**, 255 (2006).
[201] Franke, D., Vos, M., Antonietti, M., Sommerdijk, N. & Faul, C. F. J. Induced supramolecular chirality in nanostructured materials: Ionic self-assembly of perylene-chiral surfactant complexes. *Chem. Mater.* **18**, 1839 (2006).
[202] Ozer, B. H., Smarsly, B., Antonietti, M. & Faul, C. F. J. DNA-analogous structures from deoxynucleophosphates and polylysine by ionic self-assembly. *Soft Matter* **2**, 329 (2006).
[203] Faul, C. F. J., Krattiger, P., Smarsly, B. M. & Wennemers, H. Ionic self-assembled molecular receptor-based liquid crystals with tripeptide recognition capabilities. *J. Mater. Chem.* **18**, 2962 (2008).
[204] Zakrevskyy, Y., Stumpe, J. & Faul, C. F. J. A supramolecular approach to optically anisotropic materials: Photosensitive ionic self-assembly complexes. *Adv. Mater.* **18**, 2133 (2006).
[205] Zakrevskyy, Y., Stumpe, J., Smarsly, B. & Faul, C. F. J. Photoinduction of optical anisotropy in an azobenzene-containing ionic self-assembly liquid-crystalline material. *Phys. Rev. E* **75** (2007).
[206] Hermans, P. H. *Contribution to the Physics of Cellulose Fibres* (Elsevier, Amsterdam, 1946).
[207] Kelley, T. W., Baude, P. F., Gerlach, C., Ender, D. E., Muyres, D., Haase, M. A., Vogel, D. E. & Theiss, S. D. Recent progress in organic electronics: Materials, devices, and processes. *Chem. Mater.* **16**, 4413 (2004).
[208] Forrest, S. R. The path to ubiquitous and low-cost organic electronic appliances on plastic. *Nature* **428**, 911 (2004).
[209] Berggren, M., Nilsson, D. & Robinson, N. D. Organic materials for printed electronics. *Nat. Mater.* **6**, 3 (2007).
[210] Braun, D. & Heeger, A. J. Visible-light emission from semiconducting polymer diodes. *Appl. Phys. Lett.* **58**, 1982 (1991).
[211] Burroughes, J. H., Bradley, D. D. C., Brown, A. R., Marks, R. N., Mackay, K., Friend, R. H., Burns, P. L. & Holmes, A. B. Light-emitting-diodes based on conjugated polymers. *Nature* **347**, 539 (1990).
[212] Muller, C. D., Falcou, A., Reckefuss, N., Rojahn, M., Wiederhirn, V., Rudati, P., Frohne, H., Nuyken, O., Becker, H. & Meerholz, K. Multi-colour organic light-emitting displays by solution processing. *Nature* **421**, 829 (2003).
[213] Tsumura, A., Koezuka, H. & Ando, T. Macromolecular electronic device - field-effect transistor with a polythiophene thin-film. *Appl. Phys. Lett.* **49**, 1210 (1986).
[214] Sirringhaus, H., Tessler, N. & Friend, R. H. Integrated optoelectronic devices based on conjugated polymers. *Science* **280**, 1741 (1998).
[215] Dimitrakopoulos, C. D. & Malenfant, P. R. L. Organic thin film transistors for large area electronics. *Adv. Mater.* **14**, 99 (2002).
[216] Klauk, H., Zschieschang, U., Pflaum, J. & Halik, M. Ultralow-power organic complementary circuits. *Nature* **445**, 745 (2007).
[217] Yu, G., Gao, J., Hummelen, J. C., Wudl, F. & Heeger, A. J. Polymer photovoltaic cells - enhanced efficiencies via a network of internal donor-acceptor heterojunctions. *Science* **270**, 1789 (1995).
[218] Brabec, C. J., Sariciftci, N. S. & Hummelen, J. C. Plastic solar cells. *Adv. Funct. Mater.* **11**, 15 (2001).
[219] Kim, J. Y., Lee, K., Coates, N. E., Moses, D., Nguyen, T. Q., Dante, M. & Heeger, A. J. Efficient tandem polymer solar cells fabricated by all-solution processing. *Science* **317**, 222 (2007).
[220] Scott, J. C. & Bozano, L. D. Nonvolatile memory elements based on organic materials. *Adv. Mater.* **19**, 1452 (2007).
[221] Ouyang, J. Y., Chu, C. W., Szmanda, C. R., Ma, L. P. & Yang, Y. Programmable polymer thin

film and non-volatile memory device. *Nat. Mater.* **3**, 918 (2004).
[222] Bozano, L. D., Kean, B. W., Beinhoff, M., Carter, K. R., Rice, P. M. & Scott, J. C. Organic materials and thin-film structures for cross-point memory cells based on trapping in metallic nanoparticles. *Adv. Funct. Mater.* **15**, 1933 (2005).
[223] Chu, C. W., Ouyang, J., Tseng, H. H. & Yang, Y. Organic donor-acceptor system exhibiting electrical bistability for use in memory devices. *Adv. Mater.* **17**, 1440 (2005).
[224] Majumdar, H. S., Baral, J. K., Osterbacka, R., Ikkala, O. & Stubb, H. Fullerene-based bistable devices and associated negative differential resistance effect. *Org. Electron.* **6**, 188 (2005).
[225] Colle, M., Buchel, M. & de Leeuw, D. M. Switching and filamentary conduction in non-volatile organic memories. *Org. Electron.* **7**, 305 (2006).
[226] Paul, S., Kanwal, A. & Chhowalla, M. Memory effect in thin films of insulating polymer and C-60 nanocomposites. *Nanotechnology* **17**, 145 (2006).
[227] Tseng, R. J., Tsai, C. L., Ma, L. P. & Ouyang, J. Y. Digital memory device based on tobacco mosaic virus conjugated with nanoparticles. *Nat. Nanotechnol.* **1**, 72 (2006).
[228] Verbakel, F., Meskers, S. C. J. & Janssen, R. A. J. Electronic memory effects in diodes from a zinc oxide nanoparticle-polystyrene hybrid material. *Appl. Phys. Lett.* **89** (2006).
[229] Verbakel, F., Meskers, S. C. J. & Janssen, R. A. J. Electronic memory effects in a sexithiophene-poly(ethylene oxide) block copolymer doped with NaCl. combined diode and resistive switching behavior. *Chem. Mater.* **18**, 2707 (2006).
[230] Yang, Y., Ouyang, J., Ma, L. P., Tseng, R. J. H. & Chu, C. W. Electrical switching and bistability in organic/polymeric thin films and memory devices. *Adv. Funct. Mater.* **16**, 1001 (2006).
[231] Tseng, R. J., Baker, C. O., Shedd, B., Huang, J. X., Kaner, R. B., Ouyang, J. Y. & Yang, Y. Charge transfer effect in the polyaniline-gold nanoparticle memory system. *Appl. Phys. Lett.* **90** (2007).
[232] Asadi, K., De Leeuw, D. M., De Boer, B. & Blom, P. W. M. Organic non-volatile memories from ferroelectric phase-separated blends. *Nat. Mater.* **7**, 547 (2008).
[233] Leong, W. L., Lee, P. S., Lohani, A., Lam, Y. M., Chen, T., Zhang, S., Dodabalapur, A. & Mhaisalkar, S. G. Non-volatile organic memory applications enabled by in situ synthesis of gold nanoparticles in a self-assembled block copolymer. *Adv. Mater.* **20**, 2325 (2008).
[234] Verbakel, F., Meskers, S. C. J., Janssen, R. A. J., Gomes, H. L., van den Biggelaar, A. J. M. & de Leeuw, D. M. Switching dynamics in non-volatile polymer memories. *Org. Electron.* **9**, 829 (2008).
[235] Waser, R. & Aono, M. Nanoionics-based resistive switching memories. *Nat. Mater.* **6**, 833 (2007).
[236] Verbakel, F., Meskers, S. C. J., Janssen, R. A. J., Gomes, H. L., Colle, M., Buchel, M. & de Leeuw, D. M. Reproducible resistive switching in nonvolatile organic memories. *Appl. Phys. Lett.* **91** (2007).
[237] Dearnaley, G., Morgan, D. V. & Stoneham, A. M. Model for filament growth and switching in amorphous oxide films. *J. Non-Cryst. Solids* **4**, 593 (1970).
[238] Pagnia, H. & Sotnik, N. Bistable switching in electroformed metal-insulator-metal devices. *Phys. Status Solidi A* **108**, 11 (1988).
[239] Laiho, A., Baral, J. K., Majumdar, H. S., Tobjork, D., Ruokolainen, J., Osterbacka, R. & Ikkala, O. Imaging and elemental analysis of polymer/fullerene nanocomposite memory devices. *Mater. Res. Soc. Symp. Proc.* **1071**, F04\04 (2008).
[240] Shekhawat, G. S. & Dravid, V. P. Nanoscale imaging of buried structures via scanning near-field ultrasound holography. *Science* **310**, 89 (2005).
[241] Midgley, P. A., Ward, E. P. W., Hungria, A. B. & Thomas, J. M. Nanotomography in the chemical, biological and materials sciences. *Chem. Soc. Rev.* **36**, 1477 (2007).
[242] Hoppe, H. & Sariciftci, N. S. Morphology of polymer/fullerene bulk heterojunction solar cells. *J. Mater. Chem.* **16**, 45 (2006).
[243] Jakobsson, F. L. E., Crispin, X., Colle, M., Buchel, M., de Leeuw, D. M. & Berggren, M. On the switching mechanism in Rose Bengal-based memory devices. *Org. Electron.* **8**, 559 (2007).
[244] Mihailetchi, V. D., van Duren, J. K. J., Blom, P. W. M., Hummelen, J. C., Janssen, R. A. J., Kroon, J. M., Rispens, M. T., Verhees, W. J. H. & Wienk, M. M. Electron transport in a methanofullerene. *Adv. Funct. Mater.* **13**, 43 (2003).
[245] Arfken, B. *Mathematical methods for physicists* (Academic Press, New York, 1970), 2nd edn.
[246] Goyette, A. & Navon, A. Two dielectric spheres in an electric field. *Phys. Rev. B* **13**, 4320 (1976).
[247] Simmons, J. G. & Verderber, R. R. New conduction and reversible memory phenomena in

thin insulating films. *Proc. R. Soc. London, Ser. A* **301**, 77 (1967).
[248] Thurstans, R. E. & Oxley, D. P. The electroformed metal-insulator-metal structure: a comprehensive model. *J. Phys. D: Appl. Phys.* **35**, 802 (2002).

Abstracts of Publications I-VI

I Self-assembly allows new opportunities to control the morphology and properties of fullerene based materials. By using the electron-accepting underivatized C_{60} and electron-donating pyridine groups of a polystyrene-*block*-poly(4-vinylpyridine), PS-*block*-P4VP, we here show the first example that charge-transfer complexation between fullerenes and block copolymers can essentially modify the self-assembled structures. The morphology of C_{60}/PS-*block*-P4VP mixture is studied in both bulk and thin films by transmission electron microscopy (TEM) and small-angle X-ray scattering (SAXS) upon casting from freshly prepared or differently aged xylene solutions. Selecting PS-*block*-P4VP that leads to hexagonal self-assembly with P4VP cylindrical cores, closely similar cylindrical structure is observed upon adding a small amount of C_{60}, when freshly prepared xylene solutions are used to cast solid bulk or thin film samples. In this case the C_{60} molecules swell the PS matrix. By contrast, spherical morphology is observed if aged xylene solutions have been used where C_{60} has slowly penetrated into the P4VP micellar cores due to charge-transfer complexation, as evidenced by UV-vis and FTIR spectroscopy. This morphological change is unexpected, as according to simple block copolymer theory selective incorporation of a small molecular species or nanoparticles within the minority block of hexagonally self-assembled cylindrical diblock copolymer system should render the morphology toward lamellar structures. This suggests that charge-transfer complexation can be relevant in considering the self-assembled structures of block copolymers and fullerenes.

II In soft materials, self-assembled nanoscale structures can allow new functionalities but a general problem is to align such local structures aiming at monodomain overall order. In order to achieve shear alignment in a controlled manner, a novel type of rheo-optical apparatus has here been developed that allows small sample volumes and in situ monitoring of the alignment process during the shear. Both the amplitude and orientation angles of low level linear birefringence and dichroism are measured while the sample is subjected to large amplitude oscillatory shear flow. The apparatus is based on a commercial rheometer where we have constructed a flow cell that consists of two quartz teeth. The lower tooth can be set in oscillatory motion whereas the upper one is connected to the force transducers of the rheometer. A custom made cylindrical oven allows the operation of the flow cell at elevated temperatures up to 200 °C. Only a small sample volume is needed (from 9 to 25 mm^3), which makes the apparatus suitable especially for studying new materials which are usually obtainable only in small quantities. Using this apparatus the flow alignment kinetics of a lamellar polystyrene-*block*-polyisoprene diblock copolymer is studied during shear under two different conditions which lead to parallel and perpendicular alignment of the lamellae. The open device geometry allows even combined optical/x-ray in situ characterization of the alignment process by combining small-angle x-ray scattering using concepts shown by Polushkin *et al.* [Macromolecules **36**, 1421, (2003)].

III Parallel orientation of smectic layers within block copolymer lamellae is thought to exist in bulk only if long alkyl spacers are used to couple the mesogens to the polymer backbone. We report here a counter example where parallel and perpendicular orientations of smectic A layers coexist in a shear aligned side chain liquid crystalline diblock copolymer bearing a short ethyl spacer. The copolymer consists of a polystyrene block and a block of poly(methyl methacrylate) with a chiral cholesteryl mesogen as a side group i.e. poly(styrene-*block*-2-cholesteryloxycarbonyloxy ethyl methacrylate). The fraction of the parallel orientation can be controlled by oscillation frequency and shear strain amplitude as evidenced by small angle X-ray scattering and transmission electron microscopy.

IV Ionic self-assembled (ISA) surfactant complexes present a facile concept for self-assembly of various functional materials. However, no general scheme has been shown to allow their overall alignment beyond local polydomain-like order. Here we demonstrate that ionic complexes forming a columnar liquid-crystalline phase in bulk can be aligned within polymer blends upon shearing, taken that the matrix polymers have sufficiently high molecular weight. We use an ISA complex of N,N'-bis(ethylenetrimethylammonium)-perylenediimide/bis(2-ethylhexyl) phosphate (Pery-BEHP) blended with different molecular weight polystyrenes (PS). Based on X-ray scattering studies and transmission electron microscopy the pure Pery-BEHP complex was found to form a two-dimensional oblique columnar phase where the perylene units stack within the columns. Blending the complex with PS lead to high aspect ratio Pery-BEHP aggregates with lateral dimension in the mesoscale, having internal columnar liquid-crystalline order similar to the pure Pery-BEHP complex. When the Pery-BEHP/PS blend was subjected to a shear flow field, the alignment of perylenes can be achieved but requires sufficiently high molecular weight of the polystyrene matrix. The concept also suggests a simple route for macroscopically aligned nanocomposites with conjugated columnar liquid-crystalline functional additives.

V We report a simple memory device in which the fullerene-derivative [6,6]-phenyl-C_{61} butyric acid methyl ester (PCBM) mixed with inert polystyrene (PS) matrix is sandwiched between two aluminum (Al) electrodes. Transmission electron microscopy (TEM) images of PCBM:PS films showed well controlled morphology without forming any aggregates at low weight percentages (<10 wt%) of PCBM in PS. Energy dispersive x-ray spectroscopy (EDX) analysis of the device cross-sections indicated that the thermal evaporation of the Al electrodes did not lead to the inclusion of Al metal nanoparticles into the active PCBM:PS film. Above a threshold voltage of <3 V, independent of thickness, a consistent negative differential resistance (NDR) is observed in devices in the thickness range from 200 to 350 nm made from solutions with 4-10 wt% of PCBM in PS. We found that the threshold voltage (V_{th}) for switching from the high-impedance state to the low-impedance state, the voltage at maximum current density (V_{max}) and the voltage at minimum current density (V_{min}) in the NDR regime are constant within this thickness range. The current density ratio at V_{max} and V_{min} is more than or equal to 10, increasing with thickness. Furthermore, the cur-

rent density is exponentially dependent on the longest tunneling jump between two PCBM molecules, suggesting a tunneling mechanism between individual PCBM molecules. This is further supported with temperature independent NDR down to 240 K.

VI The working principles of thin film organic memory devices remain debated and tunability has been less presented. We show that the nanostructure of [6,6]-phenyl-C61-butyric acid methyl ester (PCBM) and polystyrene (PS) allows facile tuning of switching behavior for low PCBM concentrations upon annealing above the glass transition temperature of PS. By increasing the PCBM concentration from 2 to 6 wt%, the switching voltage from OFF to ON-state during the first voltage sweep systematically decreases. In subsequent voltage sweeps negative differential resistance effect is observed. Above ca. 7 wt%, chains of PCBM clusters couple the electrodes which leads to ohmic behavior.

ISBN 978-951-22-9814-3
ISBN 978-951-22-9815-0 (PDF)
ISSN 1795-2239
ISSN 1795-4584 (PDF)